NBSIR 77-861

A RELATIVELY SHORT CYLINDRICAL BROADBAND ANTENNA WITH TAPERED RESISTIVE LOADING FOR PICOSECOND PULSE MEASUREMENTS

Motohisa Kanda

Electromagnetics Division
Institute for Basic Standards
National Bureau of Standards
Boulder, Colorado 80302

August 1977

NBSIR 77-861

A RELATIVELY SHORT CYLINDRICAL BROADBAND ANTENNA WITH TAPERED RESISTIVE LOADING FOR PICOSECOND PULSE MEASUREMENTS

Motohisa Kanda

Electromagnetics Division
Institute for Basic Standards
National Bureau of Standards
Boulder, Colorado 80302

August 1977

U.S. DEPARTMENT OF COMMERCE, Juanita M. Kreps, Secretary
Sidney Harman, Under Secretary
Jordan J. Baruch, Assistant Secretary for Science and Technology

NATIONAL BUREAU OF STANDARDS, Ernest Ambler, Acting Director

CONTENTS

A RELATIVELY SHORT CYLINDRICAL BROADBAND ANTENNA WITH TAPERED RESISTIVE LOADING FOR PICOSECOND PULSE MEASUREMENTS*

Motohisa Kanda

A relatively short cylindrical antenna with continuously tapered resistive loading has been studied for the purpose of picosecond pulse and extremely broadband CW measurements. The antenna considered is a non-conducting (glass) cylinder with continuously deposited, varying-conductivity, resistive loading. The current distributions on the antenna were numerically calculated using the method of moments. Using these current distributions, other quantities, such as input impedance, near-field and far-field radiation patterns, and radiation efficiency, were also numerically calculated and compared with the results using Wu-King's approximate current distribution. Agreement is relatively good except at high frequencies, $kh > \frac{\pi}{2}$, where the method of moment appears to give better results. To verify the theoretical results, several resistively loaded antennas were fabricated, and their picosecond pulse and extremely broadband CW receiving characteristics were analyzed for the frequency range between 5 kHz and 5 GHz. The experimental results indicate excellent linear amplitude and phase response over the frequency range. This provides the unique capability of this antenna to measure fast time-varying electromagnetic fields with minimal pulse-shape distortion due to nonlinear amplitude or phase characteristics.

Key words: Broadband antenna; measurements; picosecond pulse; resistive loading, the Method of Moments.

I. INTRODUCTION

Electromagnetic interference (EMI) measurements are one of the most complicated and sophisticated measurements that challenge technology today since some devices and systems are much more susceptible to short-duration impulse interference than common CW interference. Therefore, a strong need exists to develop an isotropic broadband small sensor to detect, record, and give an alarm for electromagnetic field strengths which exceed predetermined hazardous levels. Antennas such as long electric dipoles, pulse-radiating planar arrays, long conical antennas, TEM horns, etc., have been considered previously for pulse measurements. However, these antennas become generally quite large, particularly at low frequencies. Besides, it is very difficult to make some of these antennas isotropic.

In 1965 Wu and King [1]* analyzed theoretically a dipole with continuous loaded complex impedance loading and predicted that the current distribution on such a dipole can be represented by an outward traveling wave if the complex impedance loading on a linear antenna is properly chosen. Shen and Wu [2] improved the theory by taking into account the step-function loading effect. More recently, a modified Fourier series solution for cylindrical transmitting antennas with tapered resistive and multiple impedance loading has been found by Taylor [3]. Following the work by Wu and King, Shen [4] and Lally and Rouch [5] have done some experimental work on a relatively long (more than 25 cm) resistively loaded antenna for CW operation.

For EMI measurements it is desirable to have a relatively short dipole (less than 10 cm) which is useful for picosecond pulse (less than 100 ps duration) measurements. Therefore, the purpose of this paper is to present theoretical and experimental analyses of a relatively short broadband antenna with continuously tapered, resistive loading for picosecond pulse measurements. In this paper, the current distributions on the resistively loaded antenna are calculated by solving the wave equation numerically using the method of moments. Using the current distribution obtained by the method of moments, other quantities of interest, such as input admittance, near-field and far-field radiation patterns, and radiation efficiency, are calculated and compared with the results calculated from Wu-King's current distribution.

---

*Figures in brackets indicate the literature references at the end of this paper.

To verify the theoretical results, several resistively loaded antennas were fabricated, and their picosecond pulse and CW receiving characteristics were examined experimentally. The picosecond pulse receiving characteristics of the resistively loaded antenna were analyzed using a time domain network analyzer with 70 ps duration impulses. CW receiving characteristics were examined using both a TEM cell [6] and a near-field extrapolation range [7] to cover the frequency range from 5 kHz to 5 GHz.

II. THEORETICAL CONSIDERATION

The antenna consists of a hollow cylinder of length, 2h, and radius, a, aligned along the z-axis and centered at the origin. It has an internal impedance of $Z^i(z)$ due to continuous complex impedance loading and carries an axial current of $I_z(z)$, which is assumed uniform around the periphery of the cylinder since the radius, a, is much less than the wavelength, λ. When the antenna is driven by a delta-function voltage V_o at $z = 0$, the axial component of the vector potential, $A_z(z)$, on the surface of the antenna satisfies the one-dimensional wave equation,

$$\left(\frac{\partial^2}{\partial z^2} + k^2\right) A_z(z) = \frac{jk^2}{\omega} [Z^i(z) I_z(z) - V_o \delta(z)], \tag{1}$$

where

$$A_z(z) = \frac{\mu_o}{4\pi} \int_{-h}^{h} I_z(z') \, K(z,z') dz' \tag{2}$$

and

$$K(z,z') \cong \frac{e^{-jk\sqrt{(z-z')^2 + a^2}}}{\sqrt{(z-z')^2 + a^2}} . \tag{3}$$

If the cylindrical antenna has a continuous complex impedance loading such that the internal impedance per unit length $Z^i(z)$ is a particular function of the position along the antenna, Wu and King [1] found that a pure outward traveling wave can exist on an antenna of finite length. That is, if

$$Z^i(z) = \frac{60 \psi}{h - |z|} , \tag{4}$$

where

$$\psi = \frac{\int_{-h}^{h} I(z')\, K(z,z')dz'}{I(z)}$$

$$\cong 2\left\{\sinh^{-1}\frac{h}{a} - C(2ka,2kh) - jS(2ka,2kh)\right\} + \frac{j}{kh}\left(1-e^{-j2kh}\right) \text{ at } z = 0, \quad (5)$$

and $C(a,x)$ and $S(a,x)$ are the generalized cosine and sine integrals, then the approximate current distribution for the one-dimensional wave equation (1) is of a traveling wave in nature,

$$I_z(z) = \frac{V_o}{60\psi(1-j/kh)}\left(1 - \frac{|z|}{h}\right) e^{-jk|z|}, \quad (6)$$

and the solution of $e^{+jk|z|}$ does not satisfy the original wave equation. Since the frequency dependence of $Z^i(z)$ appears only in ψ in the form of a logarithm, the antenna has much broader frequency characteristics than an antenna with lumped resistors located at quarter-wavelengths from the ends [8].

It should be noted, however, that the loading given by (4) is a complex impedance, since the constant ψ is a complex number. As will be shown later in Figs. 7(a) and 7(b), the real part of ψ is independent of frequency, and the imaginary part of ψ is negative and proportional to frequency. For this reason, it is not possible to realize the loading given by (4) using passive elements.

In the present study, a relatively short cylindrical antenna with continuously tapered resistive loading has been studied for the purpose of pulse and extremely broadband CW measurements. The current distrubution on the resistively loaded antenna for different frequencies is calculated by solving the one-dimensional wave equation given in (1) numerically using the method of moments [9]. To simplify the integral equation, it is assumed that a wire radius, a, is much smaller than a wavelength, λ, $a << \lambda$, so that the current can be considered to flow in a filament along the z-axis rather than on the surface of a cylinder. To permit a solution for the current distribution, suitable testing functions and basis functions for expansion are defined. Here we choose piecewise linear testing functions and employ

piecewise constant basis functions for expansion to solve for the current distribution on the resistively loaded antenna. Other choices of testing functions and basis functions for expansion are, of course, possible; e.g., piecewise constant, piecewise linear, piecewise sinusoidal, etc. Combinations other than piecewise linear testing functions and piecewise constant basis functions for expansion of the current might lead to better convergence. It is beyond the scope of this paper to discuss the convergence of series representations using a different combination of testing functions and basis functions for expansion. A detailed discussion on the subject is given by Butler [10].

Applying the moment method technique to the one-dimensional wave equation, the set of the wave equation may be written in matrix form as [11]

$$[V] = [Z]\,[I] \tag{7}$$

where

$$Z_{m,n} = j\,\frac{\omega}{k^2}\,\frac{1}{\Delta}\,\frac{\mu_o}{4\pi}\int_{\xi_n - \frac{\Delta}{2}}^{\xi_n + \frac{\Delta}{2}} \left[K(z_{m+1},z') - 2\left(1 - \frac{(k\Delta)^2}{2}\right) K(z_m,z') + K(z_{m-1},z')\right] dz'$$

$$+ \Delta \cdot Z^m(z_m) P_n(z_m) \tag{8}$$

and the $P_n(z_m)$'s are the basis functions used for the expansion of current, i.e., piecewise constant in this case, and $\Delta = z_m - z_{m-1}$. [V] is the voltage excitation matrix. The elements of the matrix [I], which give the current distribution, may then be obtained by solving the matrix equation.

The numerical solutions using the method of moments and the analysis based on the approximations by Wu and King have been applied to the resistively loaded antenna. In the method of moments the current distributions are calculated by subdividing the dipole into 61 subsections. In order to observe the convergence of the series representation for current on the dipole, a numerical solution with 121 subsections was examined. The results indicate that the convergence is very good for a numerical solution with 61 subsections.

III. FABRICATION OF CONTINUOUSLY TAPERED RESISTIVE LOADED ANTENNAS

The resistive antenna elements are made by depositing a linearly tapered thin film alloy on a glass rod. This alloy consists of 74.50% nickel, 20% chromium, 2.75% aluminum, and 2.75% copper, and has a relatively high resistivity of 133 μΩ-cm and a very low temperature coefficient of ± 0.00002/°C. A glass rod, 7.5 cm long and 0.254 cm in diameter, was chosen as a substrate for the deposited element. This becomes a quarter-wave monopole, $kh = \frac{\pi}{2}$, at 1 GHz. For a dipole configuration, a 15 cm long glass rod is used as a substrate for the deposited element. Once the antenna dimensions are determined, the desired resistive loading profile is calculated using (4). The desired resistive loading profile, which turns out to be a relatively weak function of frequency, is calculated at 1 GHz and is shown in Fig. 1. Here the constant ψ in (5), the ratio of the vector potential to the current along the antenna, which is in general complex, is assumed to be real by taking the absolute value of the complex constant ψ. Typically, the resistive loading required is about 5 kΩ/m at the driving point, about 10 kΩ/m at the midpoint, and infinite at the end of the antenna. Knowing the resistivity of the alloy used, i.e., 133 μΩ-cm, it is possible to calculate the required thin film thickness of the alloy, which is shown in Fig. 2. Typically, the thickness of the thin film alloy is about 24 nm at the driving point, 10 nm at the midpoint, and zero at the end of the antenna.

The 15 cm long glass rod was placed in the belljar tilted at an angle. The tilt angle is adjusted to obtain the proper resistive loading profile. The line source of the depositing alloy is used so that the resistive loading profile has a dependence of inverse distance, rather than a dependence of inverse distance squared for the point source of a depositing alloy. The photograph of the resistively loaded monopole antenna is shown in Fig. 3.

IV. COMPARISON BETWEEN MOMENT METHOD SOLUTIONS AND WU-KING APPROXIMATE SOLUTIONS

First, the current distributions on the resistively loaded antenna were calculated using both the method of moments and the Wu-King approximation. These results were compared with the experimental results. Once the current distributions were found, all other antenna characteristics, such as input admittance, near-field and far-field radiation patterns, and

radiation efficiency, were then calculated. In this section, these antenna characteristics are calculated from the current distributions obtained by both the method of moments and the Wu-King approximation, and these are in turn compared with the experiments.

A. Current Distribution

The magnitude and the phase of the current distributions on the resistively loaded antenna are calculated using both the method of moments and the Wu-King approximation and are shown in Figs. 4(a) and 4(b) for different frequencies. The experimental results of the current distribution at 1 GHz are also shown in Fig. 4(b). The current distribution measurements were made using a 1 cm diameter loop with a beam lead Schottky diode as shown in Fig. 5. High resistance, 40 MΩ per meter, lines were used in order to correct the loop to minimize distortion of both the field and the interaction with the loop antenna. The combination of resistors and capacitors forms a low pass filter to prevent rf interaction between the loop antenna and the dc measurement devices. Generally, at frequencies below 1 GHz, $kh < \frac{\pi}{2}$, the agreement between the moment method results, the Wu-King approximate solutions, and the experimental results is extremely good. However at frequencies above 1 GHz, $kh \geq \frac{\pi}{2}$, the discrepancies between them are great, and the experimental results on current distributions agree well with the results obtained by the method of moments.

B. Driving Point Admittance

The driving point admittance using the current distribution was obtained by both the method of moments and the Wu-King approximation and is compared with the experimental results. The driving conductance and the driving susceptance of the antenna are respectively shown in Fig. 6(a) and Fig. 6(b). Using the Wu-King approximation, the driving point admittance is given by

$$Y_o = \frac{1}{60\ \psi}\ \frac{1}{1 - j/kh}\ . \tag{9}$$

The experimental results were obtained by using an impedance bridge for the frequency range from 10 MHz to 300 MHz and an automatic network analyzer for the frequency range from 100 MHz to 18 GHz. The agreement between theory and experiments is relatively good except at frequencies above 1 GHz, $kh > \frac{\pi}{2}$. At frequencies below 1 GHz, $kh < \frac{\pi}{2}$, the impedance of the resistively loaded antenna is a resistance of 240 Ω and a capacitance of 0.08 pF in series configuration.

C. ψ

The ratio, ψ, of vector potential to current along an antenna is calculated by using both the current distribution from the method of moments and the Wu-King approximation. The real and imaginary parts of ψ are, respectively, shown in Figs. 7(a) and 7(b). At low frequencies below 1 GHz, $kh < \frac{\pi}{2}$, the agreement is very good between the ratio ψ calculated from the current distributions by the method of moments and that calculated from the current distributions by the Wu-King approximation. At high frequencies above 1 GHz, $kh > \frac{\pi}{2}$, the discrepancy is large, mainly due to the fact that the current distributions by the Wu-King approximation are not sufficiently accurate.

It is found from Figs. 7(a) and 7(b) that the ratio, ψ, of vector potential to current along an antenna is a very slowly varying function of frequency, since the frequency dependence of ψ in the approximate formula given in (5) appears only in the form of a logarithm. Therefore, the resistive loading profile $Z^i(z)$ given in (4) and the current distribution $I_z(z)$ given in (6) have a very weak frequency dependence, which results in the broadband characteristics.

D. Near-field and Far-field Radiation Patterns

The electric field of the resistive loaded antenna for both the near-field and the far-field regions is rigorously given by

$$E_\theta(r) = j\omega \sin\theta A_z$$

$$= \frac{j\omega\mu_o \sin\theta}{4\pi} \int_{-h}^{h} I_z(z') \frac{e^{-jk\sqrt{r^2+z'^2+2rz'\cos\theta}}}{\sqrt{r^2+z'^2+2rz'\cos\theta}} dz' . \qquad (10)$$

This integration is carried out numerically using the current distribution $I_z(z)$ obtained by the method of moments.

Using the current distribution given by the Wu-King approximation, the electric fields for both the near-field and the far-field regions are also calculated using (10) with the current distribution given in (6). In the far-field region, the electric field can be calculated analytically, yielding [1]

$$E_\theta^f(r) = \frac{jV_o}{\psi(1-j/kh)} \cdot \frac{F(kh,\theta)}{r} \tag{11}$$

where

$$F(kh,\theta) = \frac{-jkh\ \sin^2\theta+(1+\cos^2\theta)-[j2\ \cos\theta\ \sin(kh\ \cos\theta)+(1+\cos^2\theta)\cos(kh\ \cos\theta)]e^{-jkh}}{kh\ \sin^3\theta} \tag{12}$$

For comparison, the near-field and the far-field radiation patterns for a metal dipole are also shown in these figures. Here, it is assumed that the current distribution on a metal dipole is sinusoidal,

$$I(z) = I_m\ \sin[k(h-|z|)]. \tag{13}$$

The electric fields for the near-field regions are calculated here using (10) with the current distribution $I_z(z)$ given in (13). At the far-field region, the integration can be carried out analytically and leads to

$$E_\theta^f(r) = I_m\ \frac{j60}{r}\ e^{-jkr}\ \left[\frac{\cos(kh\ \cos\ \theta)\ -\ \cos\ kh}{\sin\ \theta}\right]. \tag{14}$$

The experiments to obtain the field radiation pattern were performed using a near-field calibration range [7] for the frequency range between 700 MHz and 5 GHz. A beam lead Schottky diode was mounted at the dipole driving point and was connected to a high common-mode rejection, high-impedance amplifier by means of high resistance, 50 kΩ per meter, lines to minimize both distortion of the field and interaction with the dipole.

The experimental results of the far-field radiation patterns are shown in Figs. 8(a), 8(b), 8(c), 8(d), and 8(e) for several frequencies along with the theoretical results. As shown in Figs. 8(a) and 8(b), at frequencies below 1 GHz, $kh < \frac{\pi}{2}$, the electric field patterns of the resistively loaded antenna are well-behaved and are very similar to those of a metal dipole with the same electrical length, h = 7.5 cm. As a frequency increases above 1 GHz, $kh > \frac{\pi}{2}$, the electric field patterns of a 15 cm long metal dipole split and result in many sidelobes as shown in Figs. 8(c), 8(d), and 8(e). However, Fig. 8(c) indicates that the 15 cm long resistively loaded dipole, $kh = \frac{\pi}{2}$ at 1 GHz, has a well-behaved electric field pattern up to 3 GHz, $kh = 3\frac{\pi}{2}$. At 5 GHz, $kh = 5\frac{\pi}{2}$, the electric field pattern of the resistively loaded dipole splits and results in sidelobes as shown in Fig. 8(d). For further reference, the electric field pattern of the resistively loaded antenna at 10 GHz, $kh = 10\frac{\pi}{2}$, is shown in Fig. 8(e). It was thus found that the 15 cm long resistively loaded dipole discloses a well-behaved electric field pattern up to 3 GHz, $kh = 3\frac{\pi}{2}$, whereas a 15 cm long metal dipole has a well-behaved electric field pattern up to 1 GHz, $kh = \frac{\pi}{2}$, as expected.

The near-zone electric field pattern is also calculated numerically for both the resistively loaded dipole and a metal dipole. The theoretical results are shown in Figs. 9(a), 9(b), and 9(c) for several frequencies. The near-zone electric field patterns are calculated and measured at 10 cm away from the dipole. In the measurements, a broadband balun or 3 dB hybrid coupler is used to match the balanced dipole to a 50 ohm unbalanced CW generator. A very short dipole with a Schottky barrier beam lead diode is used to probe near-field radiation patterns. At frequencies below 1 GHz, $kh < \frac{\pi}{2}$, near-field radiation patterns as shown in Figs. 9(a) and 9(b) for both the resistively loaded dipole and a metal dipole are very similar to far-field radiation patterns. However, at frequencies above 1 GHz, $kh > \frac{\pi}{2}$, the near-zone electric field pattern of the resistive loaded antenna splits and results in sidelobes as shown in Fig. 9(c). The agreement between theory and experiments is quite good as indicated in Fig. 9(b).

E. Radiation Efficiency

An obvious concern for a resistively loaded antenna is the reduced radiation efficiency of such antennas. The radiation efficiency is defined as the ratio of the total power radiated by an antenna to the net power

accepted by the antenna [12]. The radiated power P_r is calculated by integrating the Poynting vector over a sphere and is given by

$$P_r = \frac{1}{2\zeta_o} \int_o^{2\pi} d\phi \int_o^{\pi} \sin\theta \cdot |E(\theta,\phi)|^2 \cdot r^2 \, d\theta \, , \tag{15}$$

where ζ_o is a free-space impedance. The dissipated power due to resistive loading is calculated by

$$P_h = 2 \int_o^h \frac{1}{2} |I(z)|^2 \, Z^i(z) dz. \tag{16}$$

Thus the radiation efficiency is given by

$$y_r = \frac{P_r}{P_h + P_r} \, . \tag{17}$$

The current distribution on the resistively loaded antenna obtained by the method of moments is used to numerically calculate the radiation efficiency, and the result is shown in Fig. 10.

In the far-field range, using the approximate current distribution given by (6), the radiated power, P_r, is given by [1]

$$P_r = \frac{2\pi V_o^2}{\zeta_o |\psi|^2 (1 + \frac{1}{k^2h^2})} \int_o^1 F^2 dy \tag{18}$$

where F is given in (12) and $y = \cos\theta$. Under the same assumption, the dissipated power P_h is also given as

$$P_h = \frac{\pi V_o^2}{\zeta_o |\psi| (1 + \frac{1}{k^2h^2})} \, . \tag{19}$$

The resultant radiation efficiency is also shown in Fig. 10. The agreement between the radiation efficiency calculated by the current distribution obtained by the method of moments and that obtained from the Wu-King current distribution is relatively good except at frequencies above 1 GHz, $kh > \frac{\pi}{2}$. At frequencies above 1 GHz, $kh > \frac{\pi}{2}$, the experimental results on the current distribution on the resistively loaded antenna agree well with the theoretical

results obtained by the method of moments. Thus, it is expected that the radiation efficiency based on the current distribution by the method of moments will give a correct value at frequencies above 1 GHz, $kh > \frac{\pi}{2}$.

V. TIME DOMAIN MEASUREMENTS FOR THE RESISTIVELY LOADED ANTENNA WITH A 50 Ω LOAD

The transients of the resistively loaded antenna were evaluated on the time domain antenna range with the Time Domain Automatic Network Analyzer (TDANA) developed by the National Bureau of Standards (NBS). The TDANA measures the time domain waveform of impulse response of the resistively loaded antenna. The time domain waveform is then digitized and stored in the minicomputer memory. By acquiring an ensemble of many waveforms, it is possible to perform signal averaging within the minicomputer to improve the signal to noise ratio in the measurements. The minicomputer then computes the spectrum amplitude from the digitized, averaged waveform using the Fast Fourier Transform (FFT).

The bottom curve of Fig. 11(a) shows the time domain waveform of the impulse from the impulse generator. The duration of the impulse is typically 70 ps, and its amplitude is about 5 to 6 volts. This impulse is transmitted through a 2.8 m long conical standard antenna and received on the resistively loaded antenna. The antenna feed points on the ground plane are separated by 1 meter. The upper curve of Fig. 11(a) shows the time domain waveform of the impulse received by the resistively loaded antenna. It should be noted how well the resistively loaded antenna can preserve the waveform of the radiated impulse field from the conical antenna. On the other hand, when a metal dipole with the same electrical length is used for receiving the same impulse, the shape of the 70 ps impulse is completely destroyed as shown in Fig. 11(b).

Using the time domain wave of the impulse from the impulse generator which is shown in the bottom curve in Fig. 11(a), the spectrum amplitude of the impulse is calculated by an FFT and is shown in Fig. 12. The spectrum amplitude is relatively flat with a nominal level of 60 dBμV/MHz to 5 GHz. Beyond 6 GHz, the spectrum amplitude drops very rapidly.

Figure 13 shows the transfer functions of a two antenna system, a conical standard antenna for transmitting and the 7.5 cm long resistively loaded monopole for receiving. The transfer function is calculated by taking an FFT on the time domain waveform of the impulse received by the resistively loaded antenna, which is shown in the upper curve of Fig. 12(a). It is found from Fig. 13 that the resistively loaded monopole has a frequency response that is flat to ± 3 dB from 200 MHz to over 5 GHz.

VI. FREQUENCY DOMAIN MEASUREMENTS FOR THE RESISTIVELY LOADED ANTENNA WITH A DIODE LOAD

A beam lead Schottky diode is mounted on the center of the resistively loaded dipole. The diode has high sensitivity, small shunt capacitance ($\sim$ 0.2 pF), low temperature dependence, high back resistance ($\sim$ 20 MΩ), and high reverse breakdown voltage ($\sim$ 3 V). High resistance, 50 kΩ per meter, lines are connected to the diode. They form a parallel-wire transmission line to minimize differential-mode noise. These high resistance transmission lines produce both little distortion of the electromagnetic field and little interaction with the resistively loaded dipole. The preamplifier with unity voltage gain is designed to provide proper sensor loading ($\sim$ 1 MΩ), precise zero adjustment, high common mode rejection ratio ($\sim$ 90 dB at dc), low drift, and low noise operation. The output from the preamplifier is read by a dc voltmeter.

The standard, uniform electromagnetic fields are established both in a TEM transmission cell [6] for the frequency range between 5 kHz and 400 MHz and in a near-field extrapolation range [7] for the frequency range between 700 MHz and 5 GHz. Figure 14 shows the required electric field in volts per meter to produce 10 mV output across the dipole.

From Fig. 14 it is determined that the frequency response of the resistively loaded antenna for the frequency range between 1 MHz and 1 GHz is extremely flat and that the ± 3 dB bandwidth for the antenna lies from 700 kHz to 2 GHz; i.e., over 3 decades.

The rolloff at the low end of the frequency is mainly due to back resistance ($\sim$ 20 MΩ) of the diode, and cutoff at the high end of the frequency is due to shunt capacitance (0.2 pF) of the diode. Limited analysis of center-loaded antennas with nonlinear loads has been done recently by Liu and Tesche [13]. More general analysis, which is particularly applicable to the present study, will be prepared and presented as the subject of a future paper.

VII. CONCLUSION

The characteristics of a relatively short, cylindrical, broadband antenna with continuous resistive loading were studied theoretically and experimentally for picosecond pulse measurements. The antenna considered is a non-conducting (glass) cylinder with continuously deposited, tapered, resistive loading. The current distribution on the resistively loaded antenna is calculated using the method of moments and compared with the Wu-King approximate formula. Experimental results indicate that the real current distribution on the resistively loaded antenna agrees with the results of the method of moments. Using the current distributions obtained both by the method of moments and the Wu-King approximation, other quantities, such as input admittance, near-field and far-field radiation patterns, and radiation efficiency, were calculated, and are also examined experimantally. These experimental results agree well with the predicted results of both methods up to 1 GHz, but agreement is better with the moment method above 1 GHz.

Time domain measurements were performed using a time domain antenna range with a time domain automatic network analyzer. The receiving characteristics of the resistively loaded antenna indicate that the radiated impulse shape of 70 ps duration is well preserved. The resistively loaded antenna has a response flat to ± 3 dB from 200 MHz to over 5 GHz.

The resistively loaded antenna with a beam lead Schottky diode load was examined. The frequency response is flat to ± 3 dB from 700 MHz to 2 GHz. With proper response shaping, the resistively loaded antenna has a potential use for the frequency range between 10 kHz and 3 GHz without distorted antenna field patterns.

The theoretical and experimental results indicate that the resistively loaded antenna processes excellent linear amplitude and phase response over the broad frequency range. This provides the unique capability of the antenna to measure fast time-varying electromagnetic fields with minimal pulse-shape distortion due to nonlinear amplitude or phase characteristics.

ACKNOWLEDGMENT

The author wishes to thank Dr. P. F. Wacker for many stimulating discussions, and B. K. Bender for computer assistance. Acknowledgment should also be extended to D. G. Melquist, A. R. Ondrejka, and T. H. Bremer for their experimental assistance, and C. K. S. Miller, F. X. Ries, and J. W. Adams for many helpful discussions and encouragement during the course of this work.

REFERENCES

[1] T.T. Wu and R.W.P. King, "The cylindrical antenna with nonreflecting resistive loading," IEEE Trans. Antennas Propagat., vol. AP-13, no. 3, pp. 369-373, May 1965. This paper was corrected by
L.C. Shen and R.W.P. King, "The cylindrical antenna with nonreflecting resistive loading," IEEE Trans. Antennas Propagat., vol. AP-13, no. 6, p. 998, Nov. 1965.

[2] L.C. Shen and T.T. Wu, "Cylindrical antenna with tapered resistive loading," Radio Science, vol. 2, no. 2, pp. 191-201, Feb. 1967.

[3] C.D. Taylor, "Cylindrical transmitting antenna: tapered resistivity and multiple impedance loading," IEEE Trans. Antennas Propagat., vol. AP-16, no. 2, pp. 176-179, March 1968.

[4] L.C. Shen, "An experimental study of the antenna with nonreflecting resistive loading," IEEE Trans. Antennas Propagat., vol. AP-15, no. 5, pp. 606-611, Sept. 1967.

[5] J.F. Lally and D.T. Rouch, "Experimental investigation of the broadband properties of a continuously loaded resistive monopole," IEEE Trans. Antennas Propagat., vol. AP-18, no. 6, pp. 764-768, Nov. 1970.

[6] M.L. Crawford, "Generation of standard EM fields using TEM transmission cells," IEEE Trans. Electromagnetic Compat., vol. EMC-16, no. 4, pp. 189-195, Nov. 1974.

[7] R.R. Bowman, "Calibration techniques for electromagnetic hazard meters; 500 MHz to 20 GHz," Nat. Bur. Stand. Internal Report 75-805, April 1976.

[8] E.E. Altshuler, "The traveling-wave linear antenna," IEEE Trans. Antennas Propagat., vol. AP-9, no. 4, pp. 324-329, July 1961.
K. Iizuka, "The traveling-wave V-antenna and related antennas," IEEE Trans. Antennas Propagat., vol. AP-15, no. 2, pp. 236-243, March 1967.

[9] R.E. Harrington, Field Computation by Moment Methods. New York: The Macmillan Company, 1968.

[10] C.M. Butler and D.M. Wilton, "Analysis of various numerical techniques applied to thin wire scatterers," IEEE Trans. Antennas Propagat., vol. AP-23, no. 4, pp. 534-540, July 1975.

[11] "Moment methods in electromagnetics," Supplementary Notes for a Short Course in Electromagnetic Theory, Department of Electrical Engineering, The University of Mississippi, Mississippi, 1975.

[12] "IEEE standard definitions of terms for antennas," IEEE Std. 145-1973, Aug. 1973.

[13] T.K. Liu and F.M. Tesche, "Analysis of antennas and scatterers with nonlinear loads," IEEE Trans. Antennas Propagat.. vol. AP-24, no. 2, pp. 131-139, March 1976.

FIGURE CAPTIONS

Fig. 1. Resistive loading profile.

Fig. 2. Required profile of thin film thickness of the alloy.

Fig. 3. Photograph of resistively loaded monopole.

Fig. 4. Current distribution on resistively loaded antenna: a) at 100 MHz, and b) at 1 GHz.

Fig. 5. Photograph of loop antenna used for current distribution measurements.

Fig. 6. Driving point admittance of resistively loaded dipole: a) driving point conductance, and b) driving point susceptance.

Fig. 7. ψ as a function of frequency: a) real part of ψ, and b) imaginary part of ψ.

Fig. 8. Far-field radiation patterns: a) at 100 MHz, b) at 1 GHz, c) at 2.5 GHz, d) at 5 GHz, and e) at 10 GHz.

Fig. 9. Near-field radiation patterns: a) at 100 MHz, b) at 1 GHz, and c) at 5 GHz.

Fig. 10. Radiation efficiency of resistively loaded antenna.

Fig. 11. Time domain impulse responses: a) resistively loaded monopole, and b) a metal monopole.

Fig. 12. Spectrum amplitude of impulse.

Fig. 13. Transfer function of two antennas: conical standard antenna for transmitting and resistively loaded monopole for receiving.

Fig. 14. Frequency response of resistively loaded antenna.

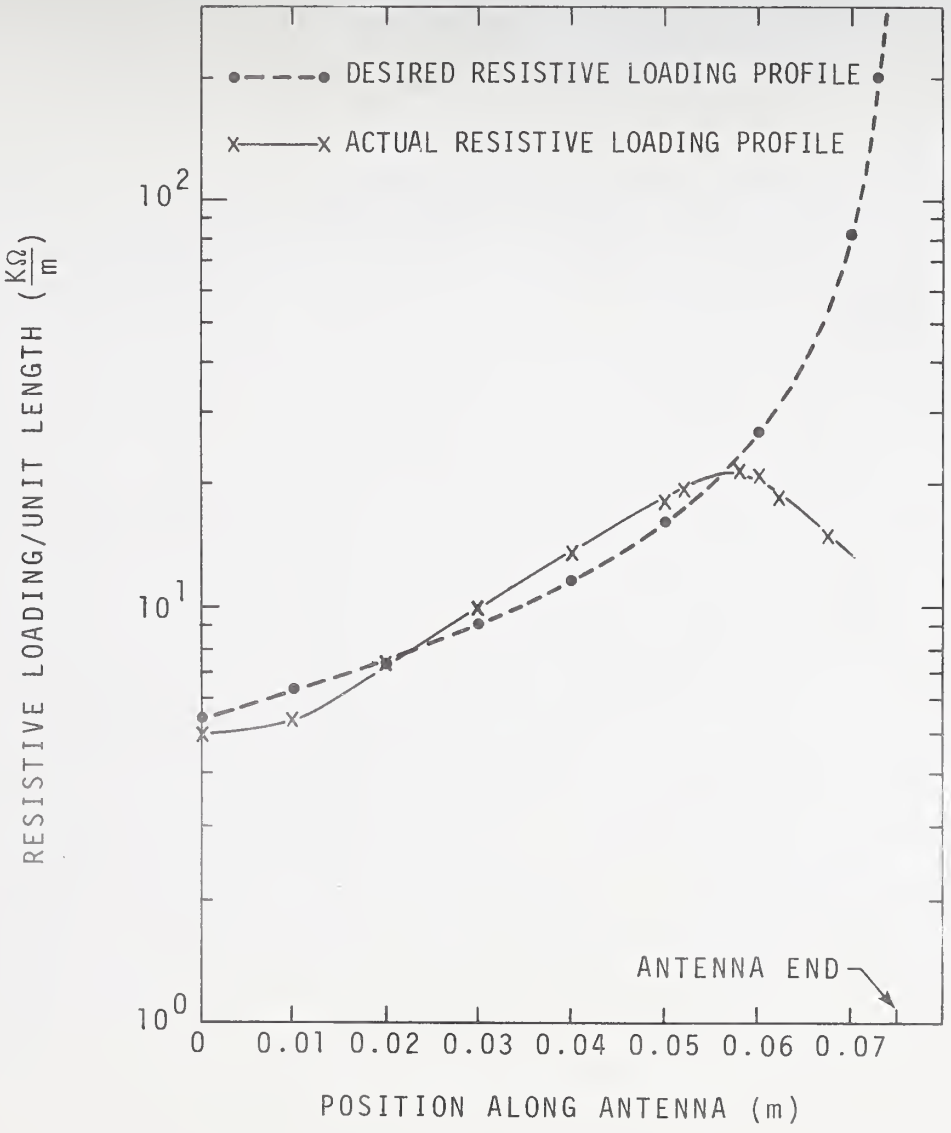

Figure 1. Resistive loading profile.

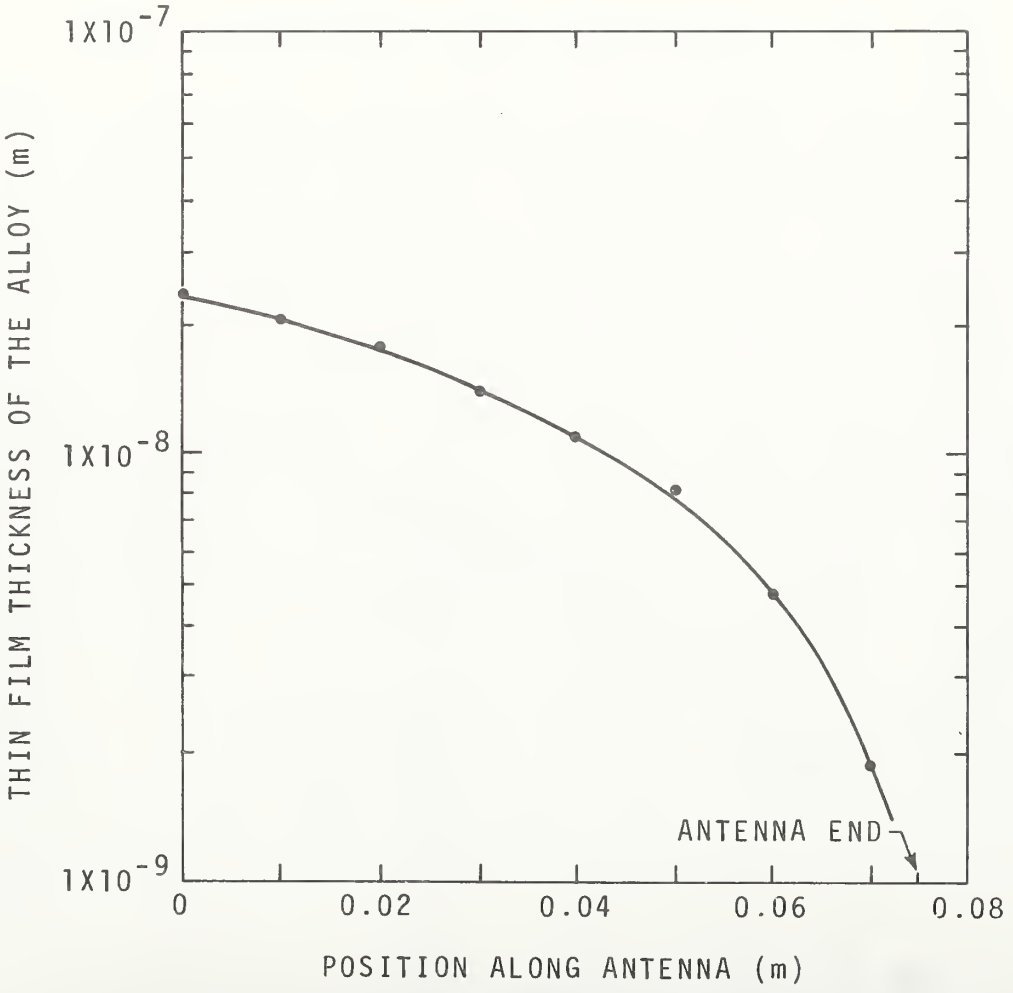

Figure 2. Required profile of thin film thickness of the alloy.

Figure 3. Photograph of resistively loaded monopole.

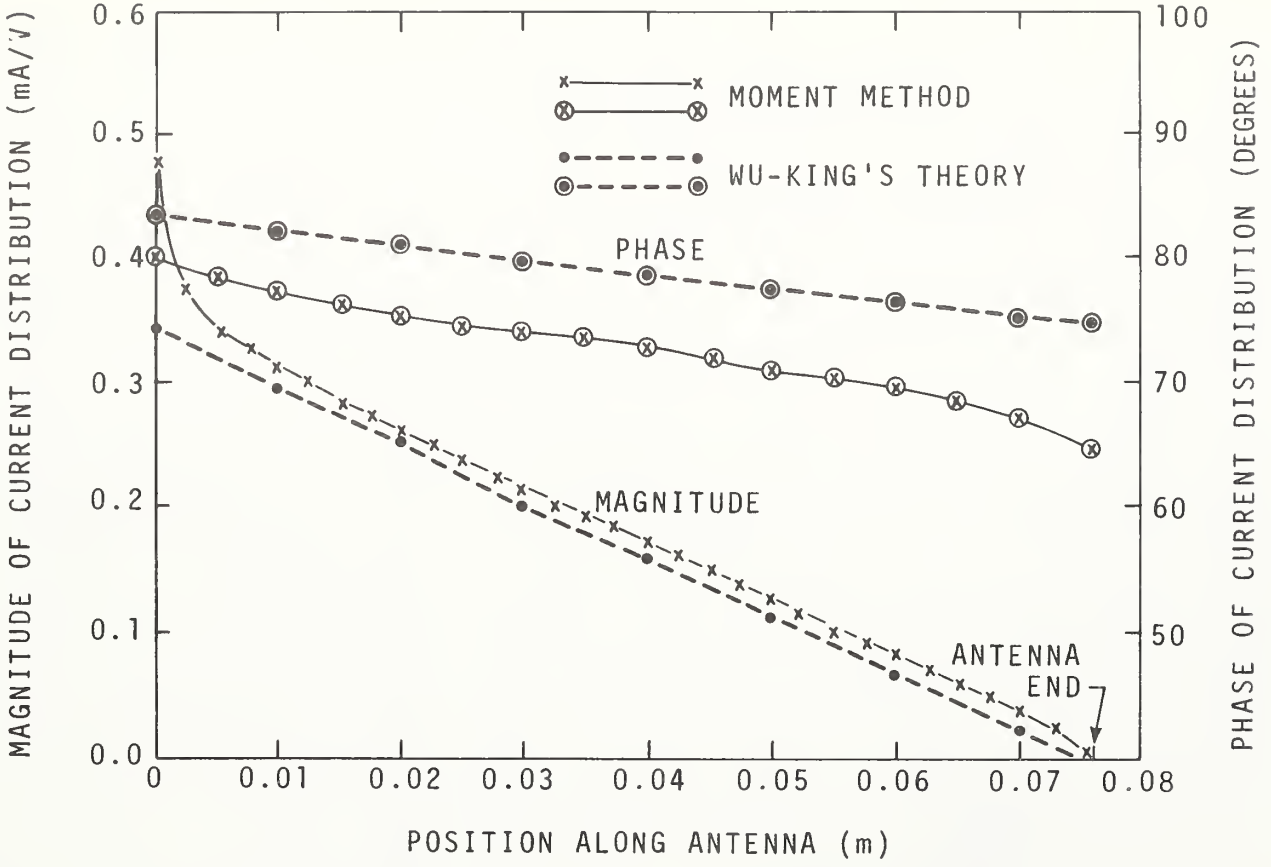

Figure 4. Current distribution on resistive loaded antenna.

a) at 100 MHz

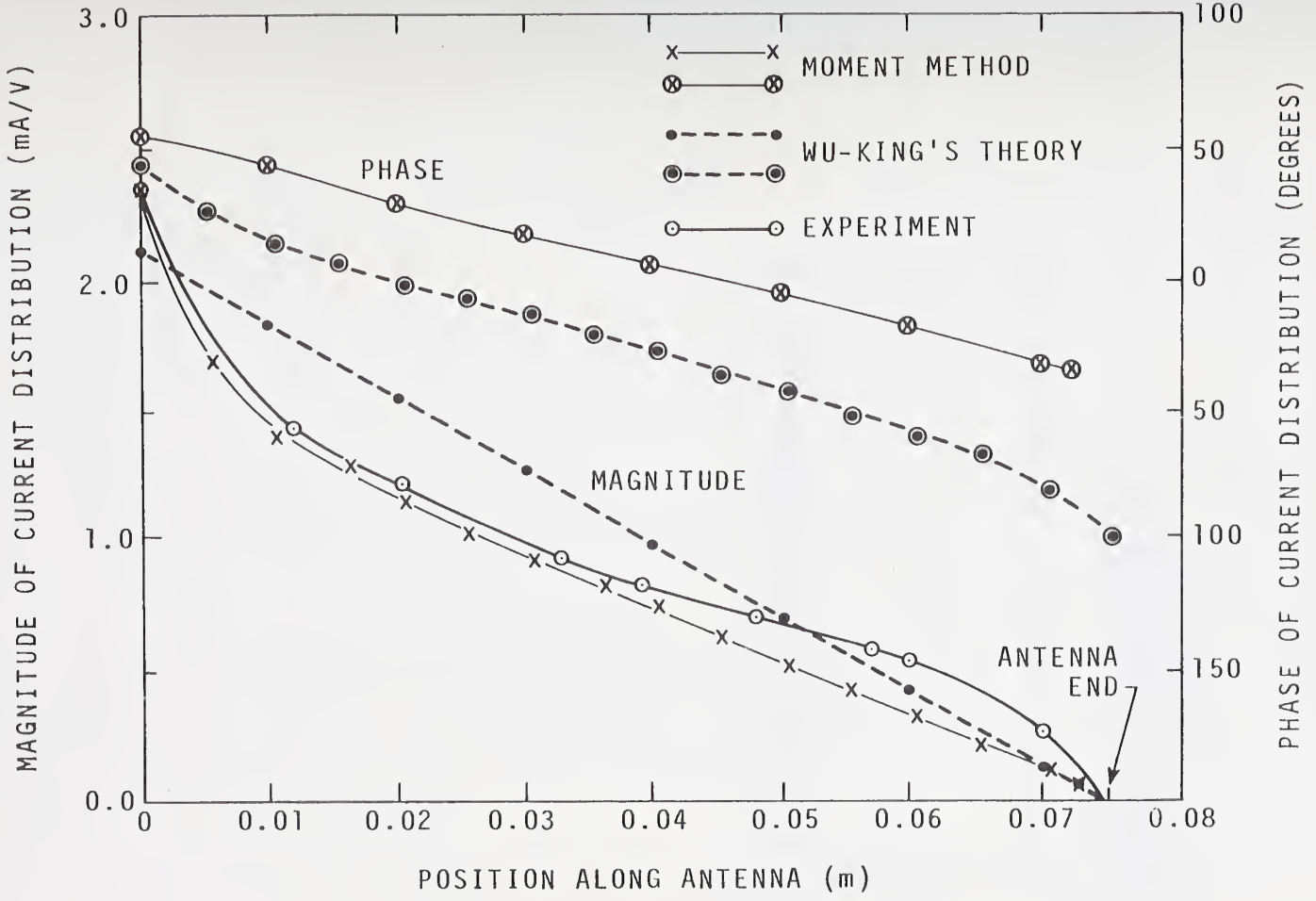

Figure 4. Current distribution on resistive loaded antenna.

b) at 1 GHz

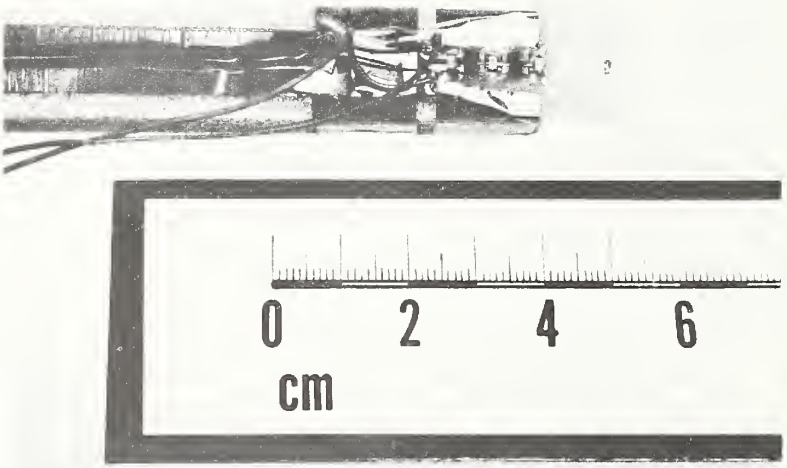

Figure 5. Photograph of loop antenna used for current distribution measurements.

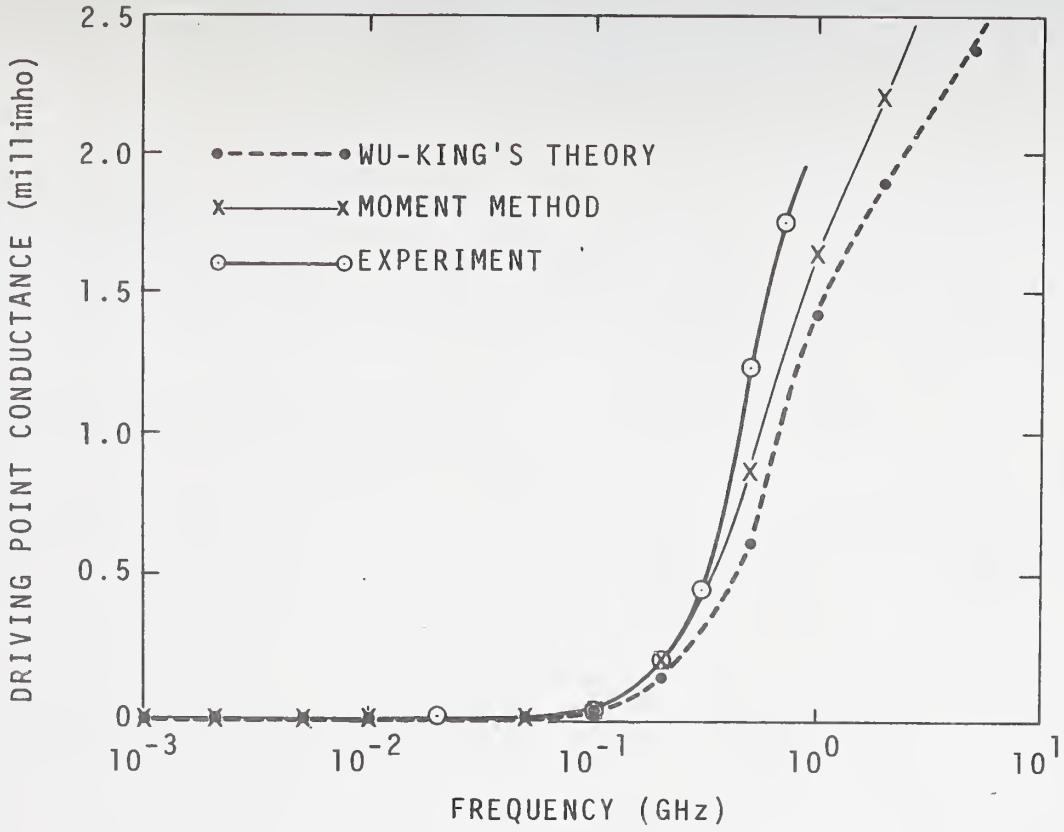

Figure 6. Driving point admittance of resistive loaded dipole.

a) driving point conductance

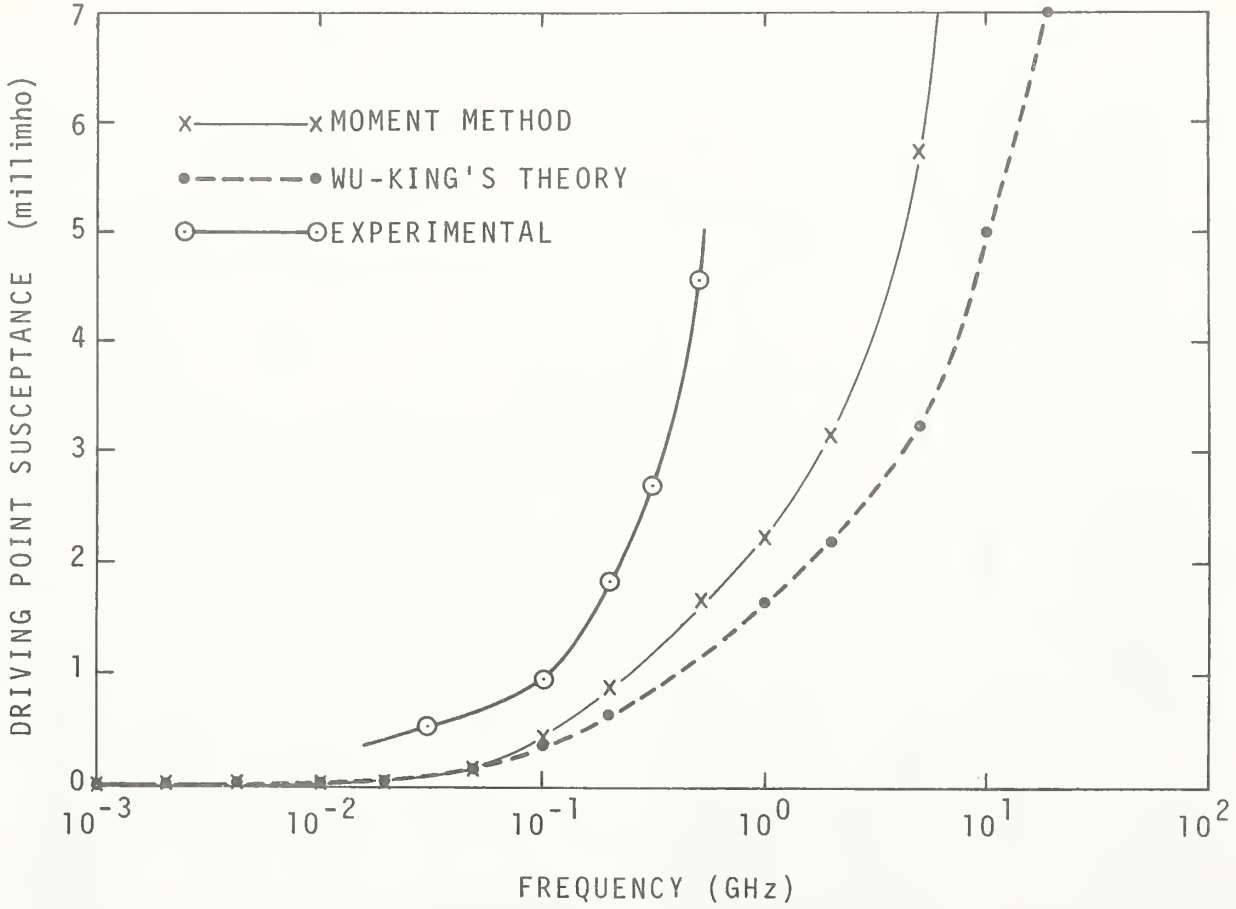

Figure 6. Driving point admittance of resistive loaded dipole.

b) driving point susceptance

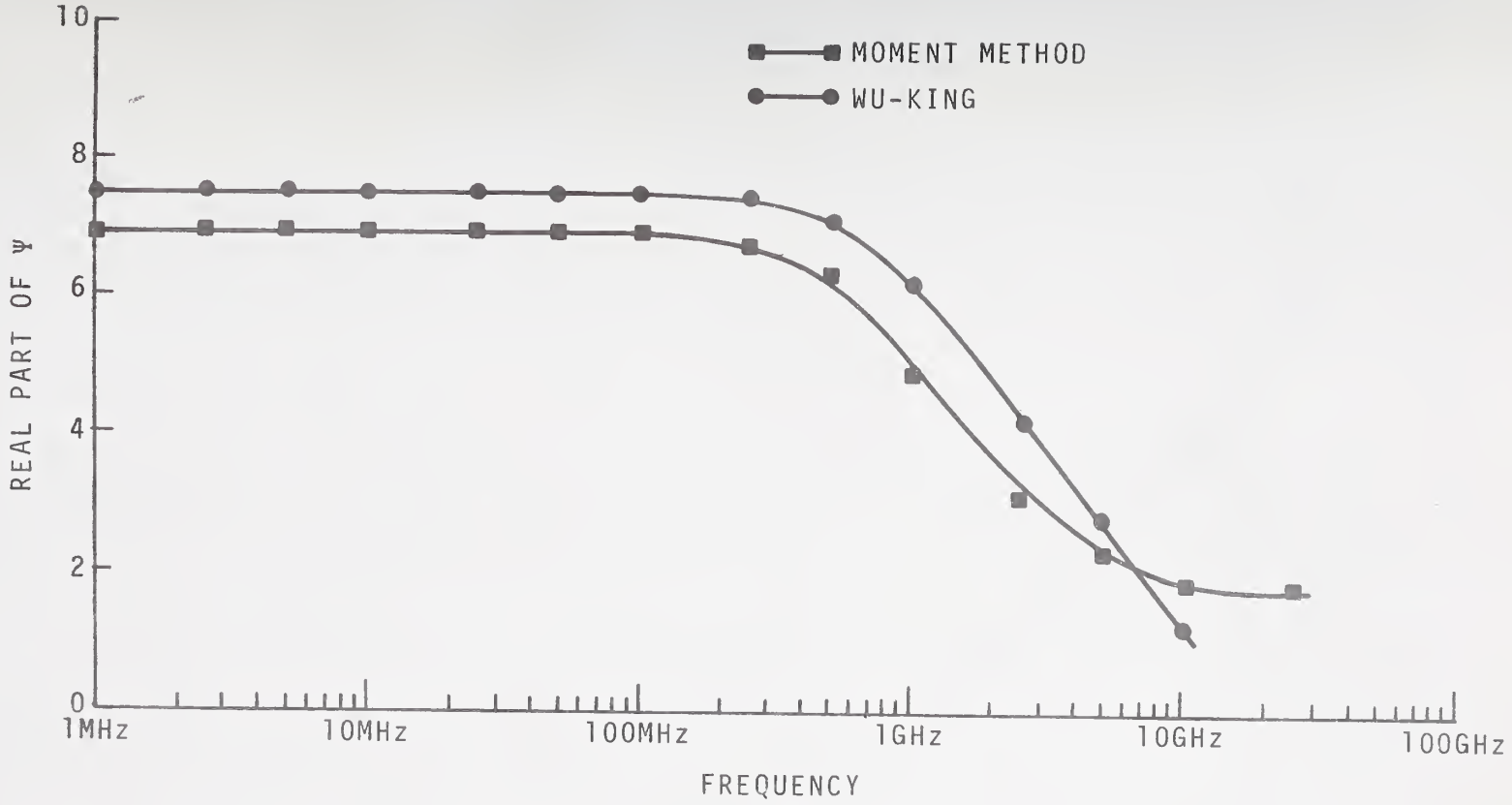

Figure 7. ψ as a function of frequency.

a) real part of ψ

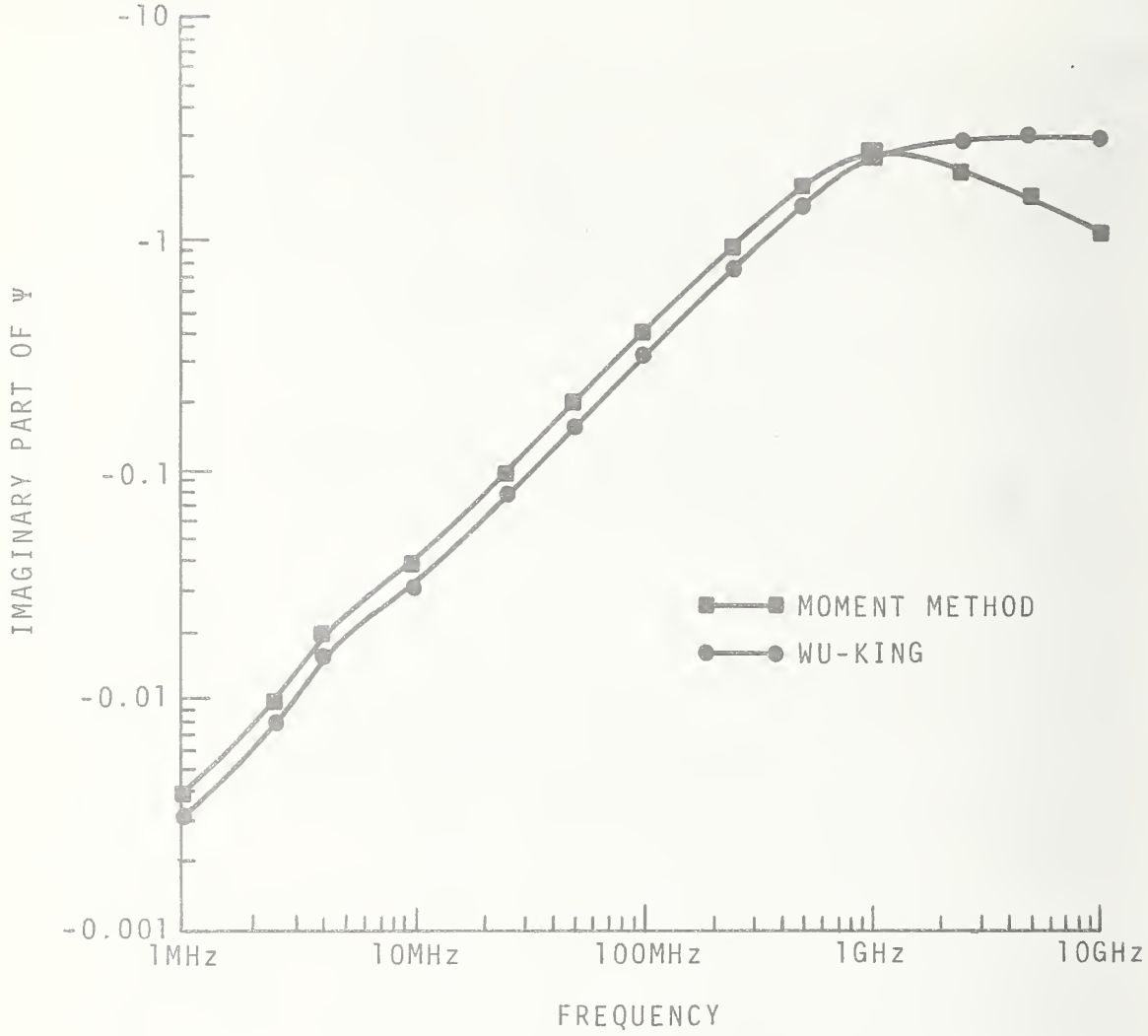

Figure 7. ψ as a function of frequency.

b) imaginary part of ψ

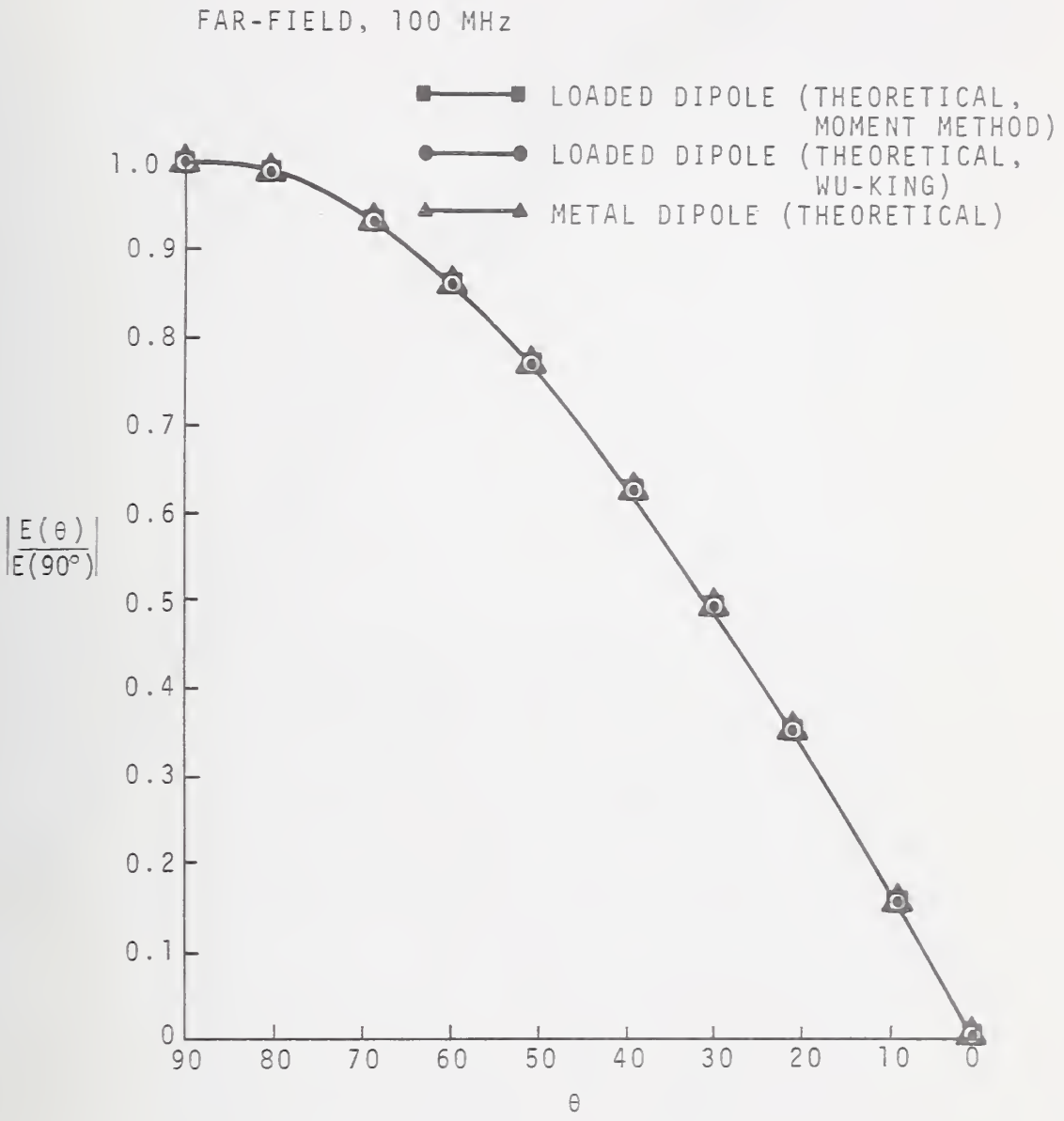

Figure 8. Far-field radiation patterns: a) at 100 MHz

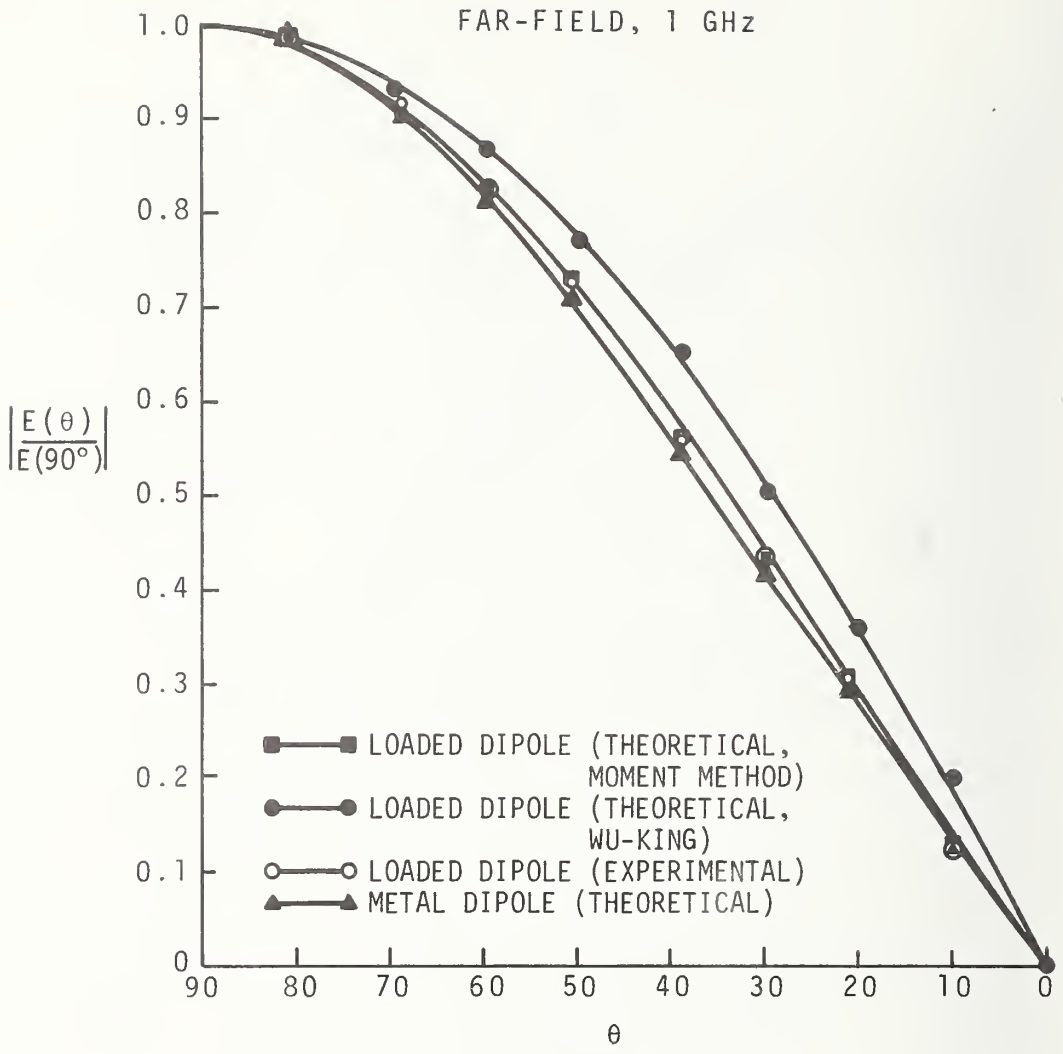

Figure 8. Far-field radiation patterns: b) at 1 GHz

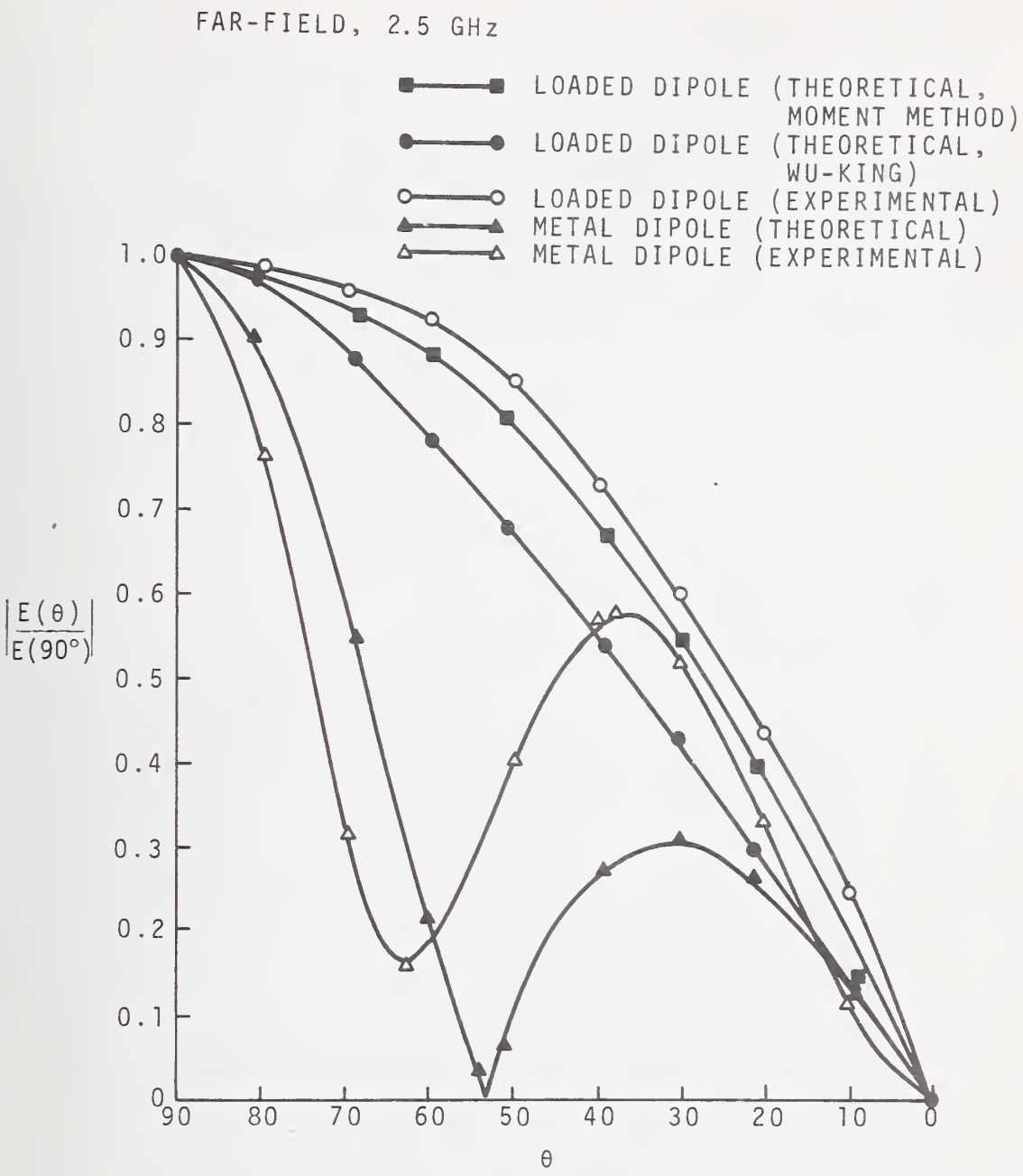

Figure 8. Far-field radiation patterns: c) at 2.5 GHz

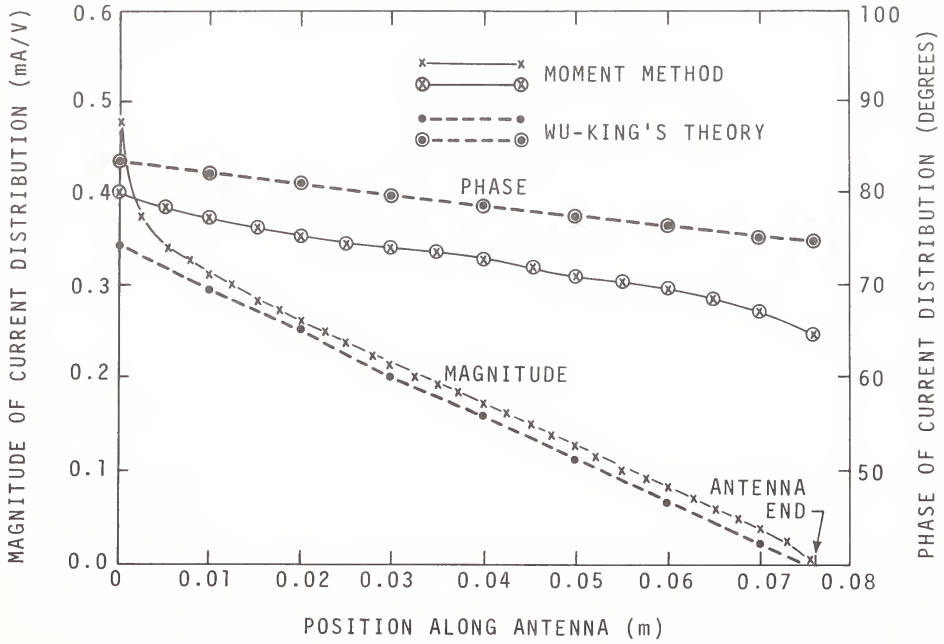

Figure 4. Current distribution on resistive loaded antenna.

a) at 100 MHz

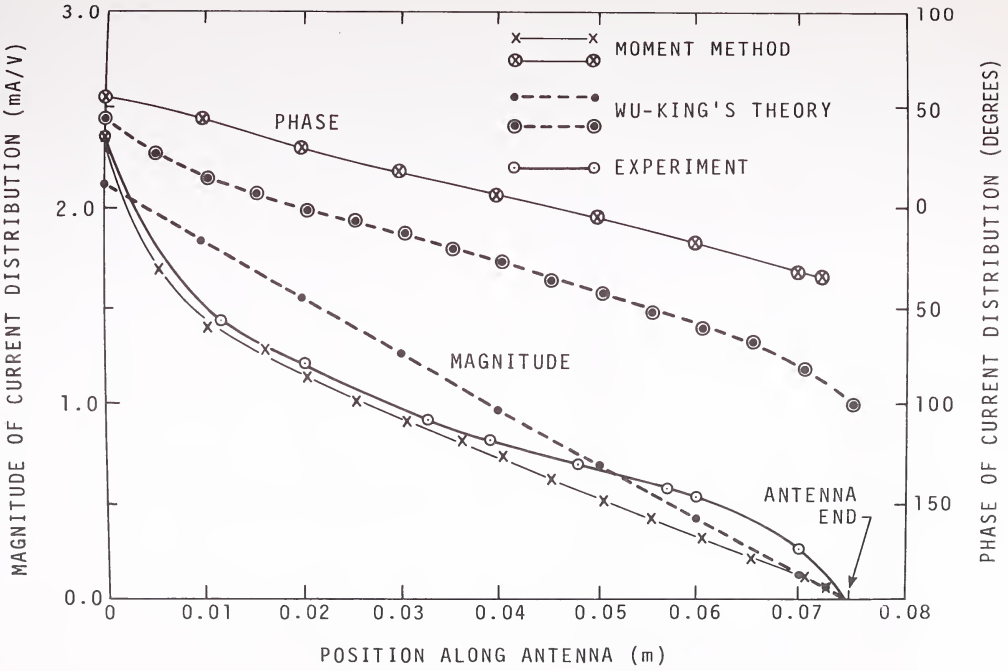

Figure 4. Current distribution on resistive loaded antenna.

b) at 1 GHz

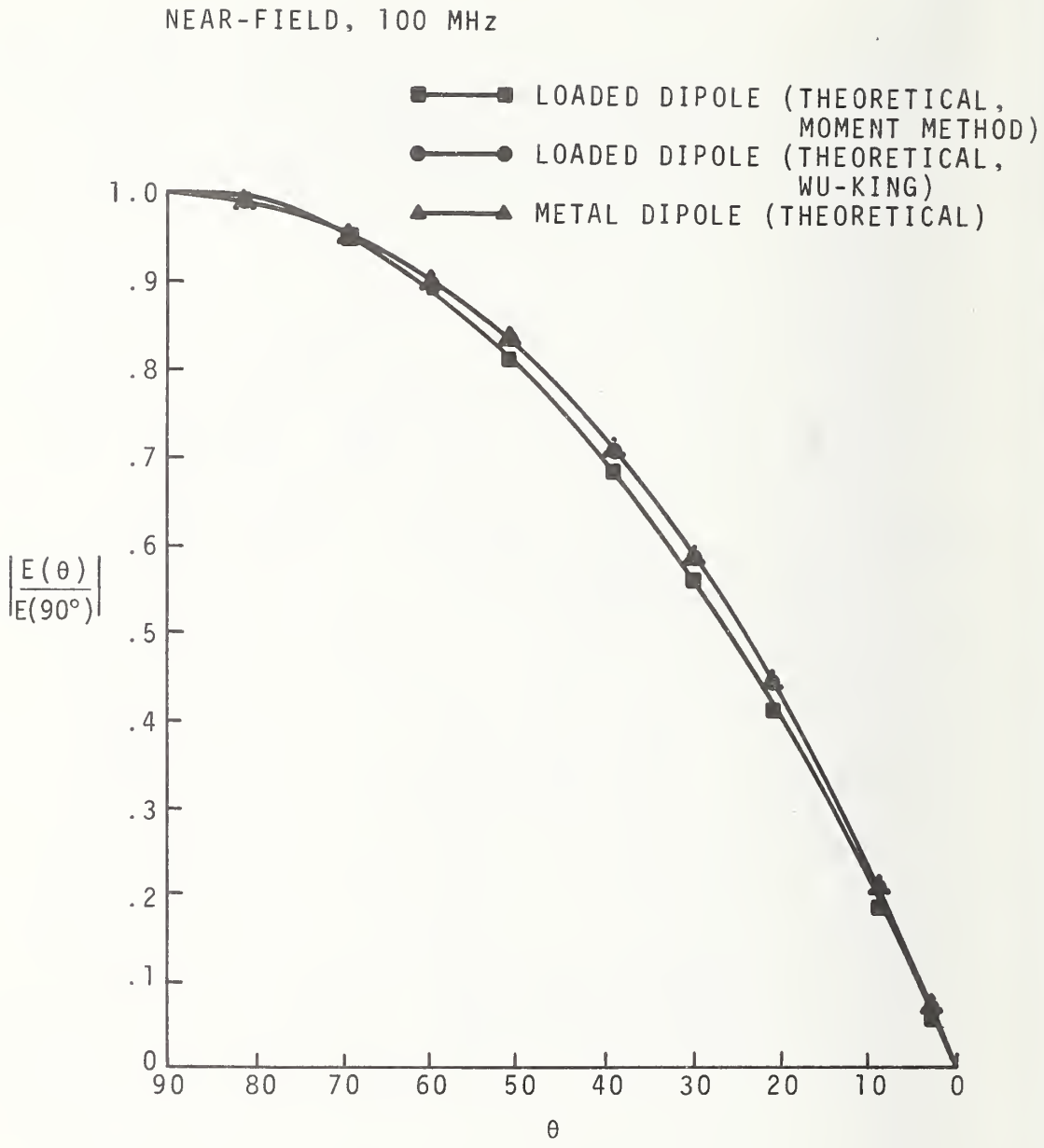

Figure 9. Near-field radiation patterns: a) at 100 MHz.

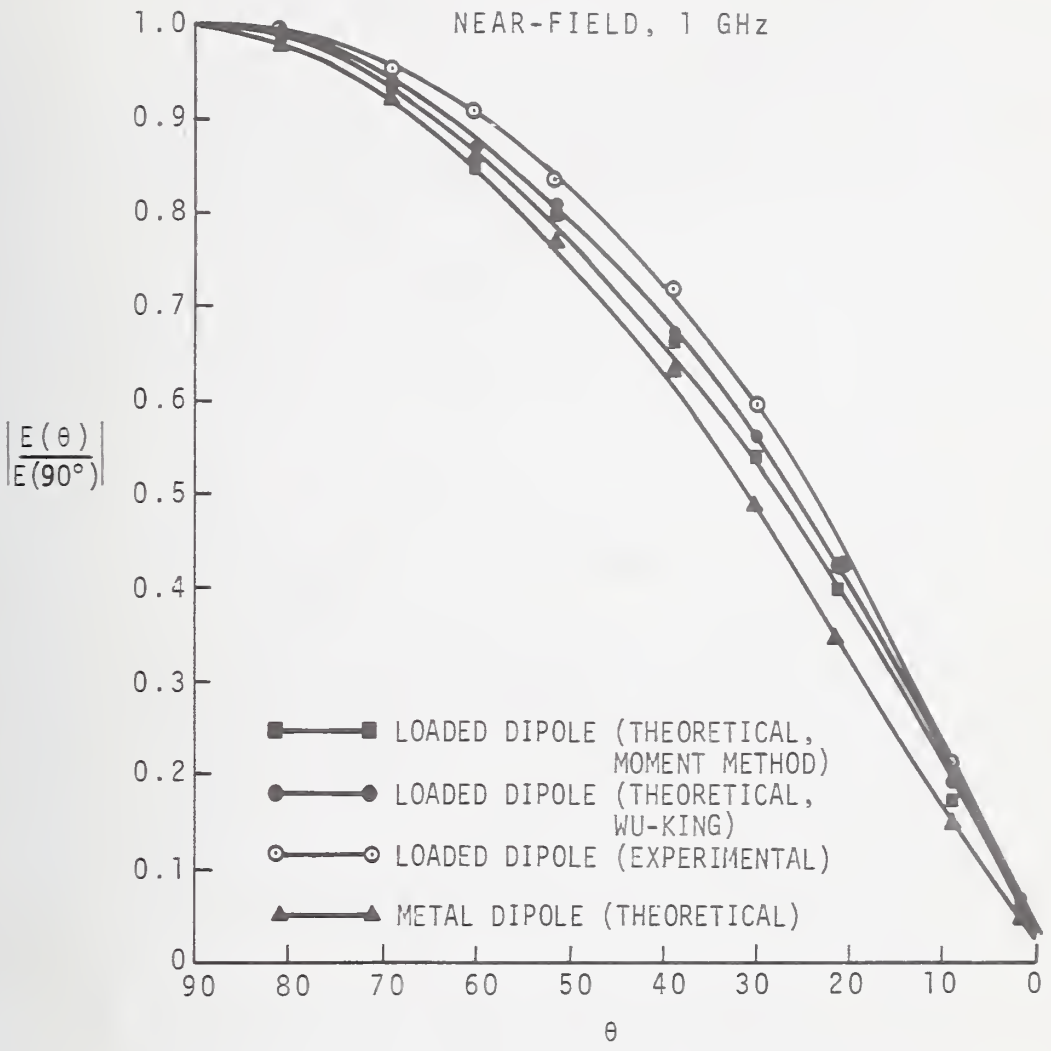

Figure 9. Near-field radiation patterns: b) at 1 GHz.

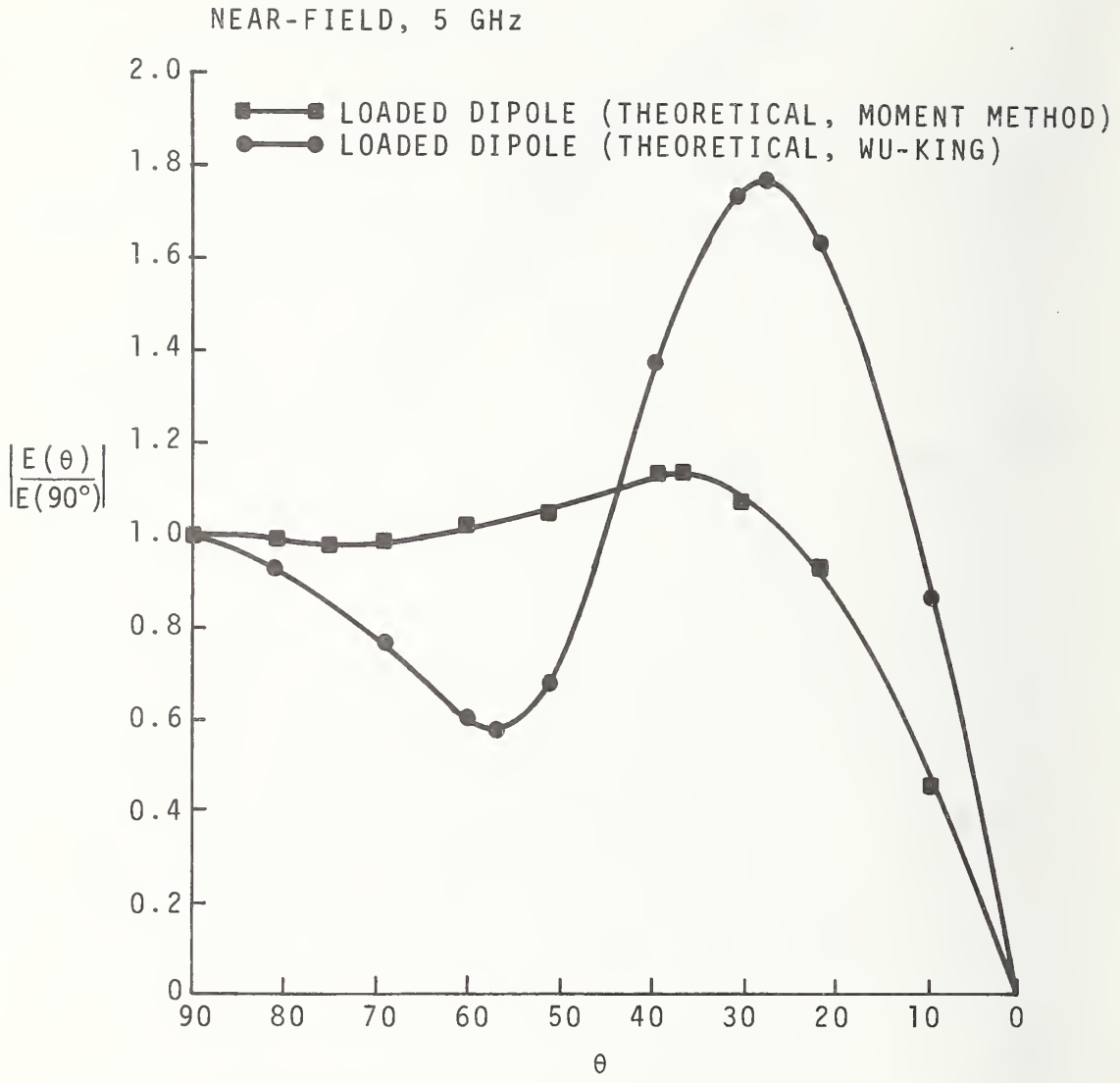

Figure 9. Near-field radiation patterns: c) at 5 GHz.

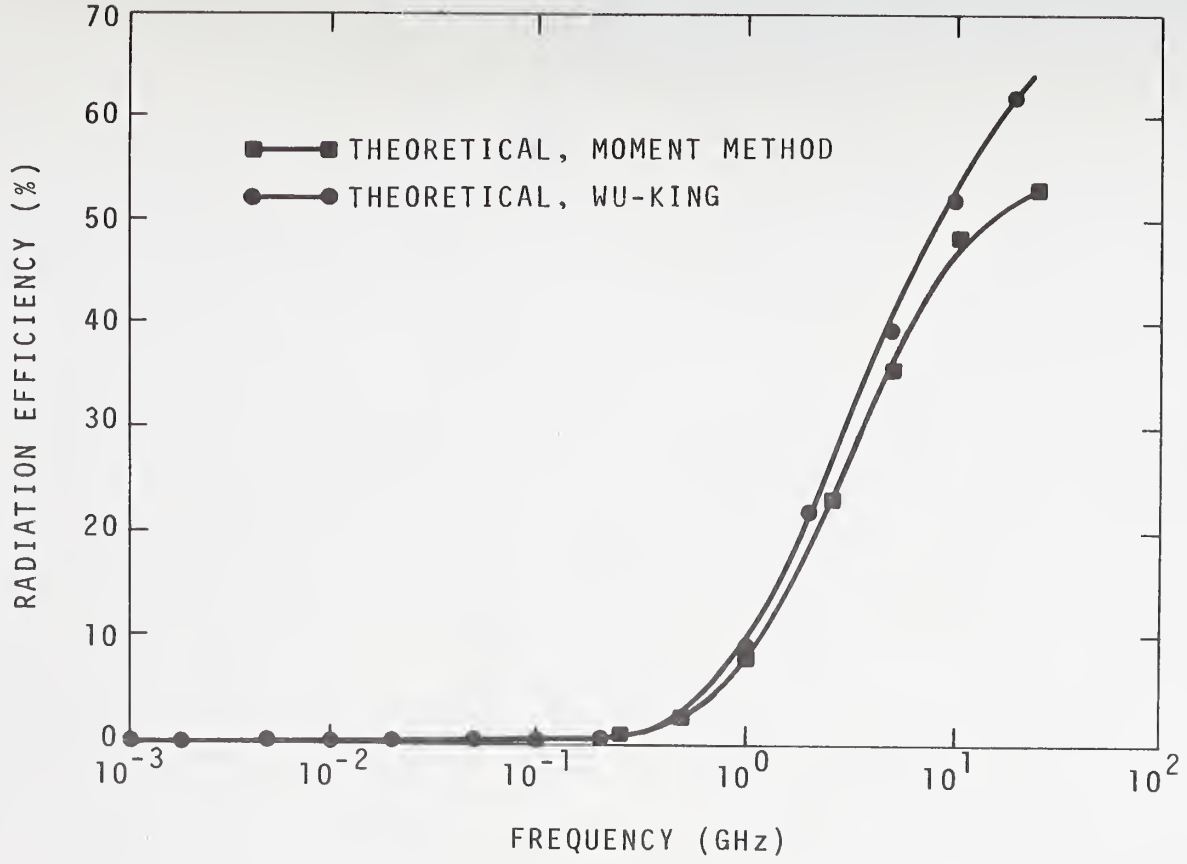

Figure 10. Radiation efficiency of resistively loaded antenna.

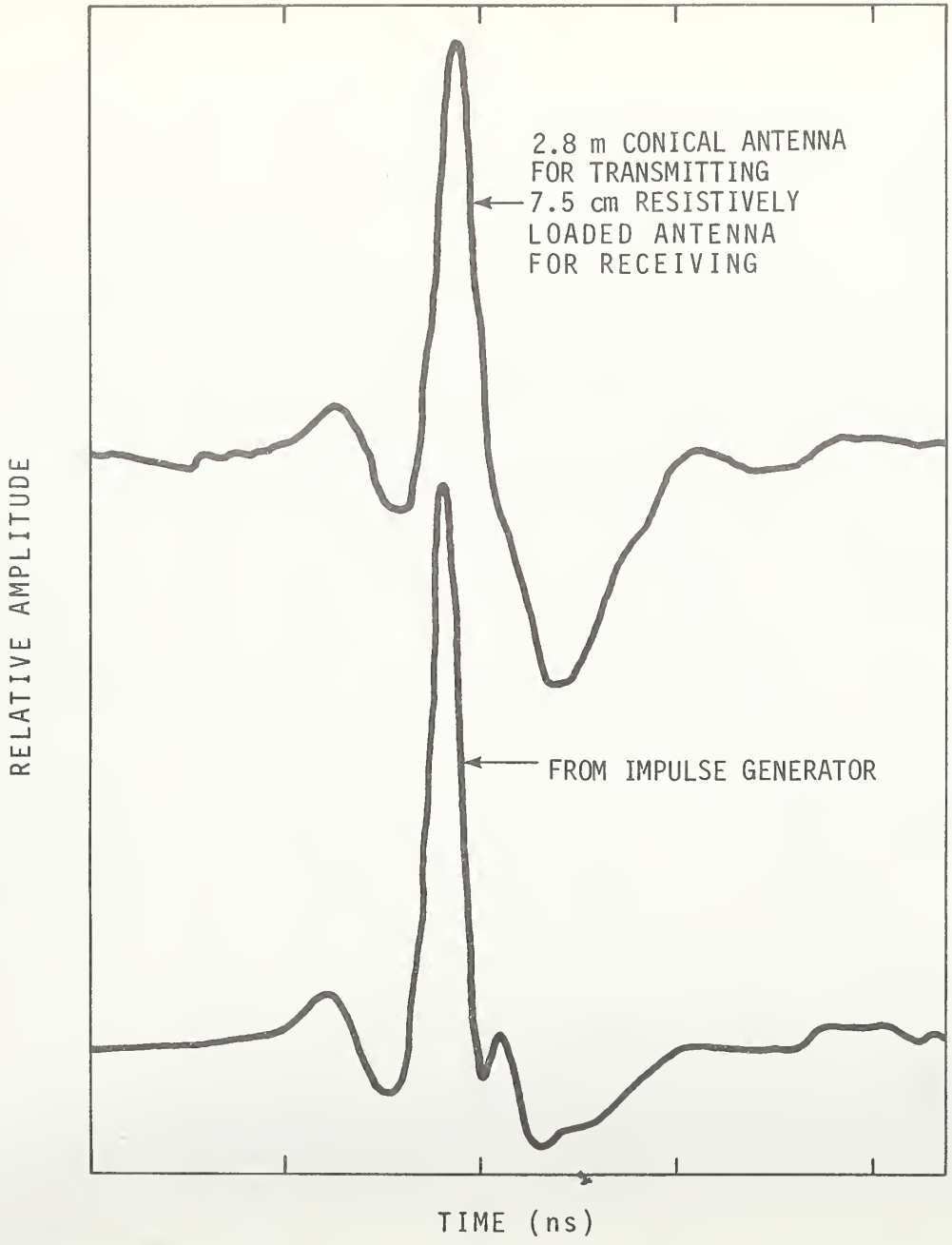

Figure 11. Time domain impulse responses.

a) resistively loaded monopole

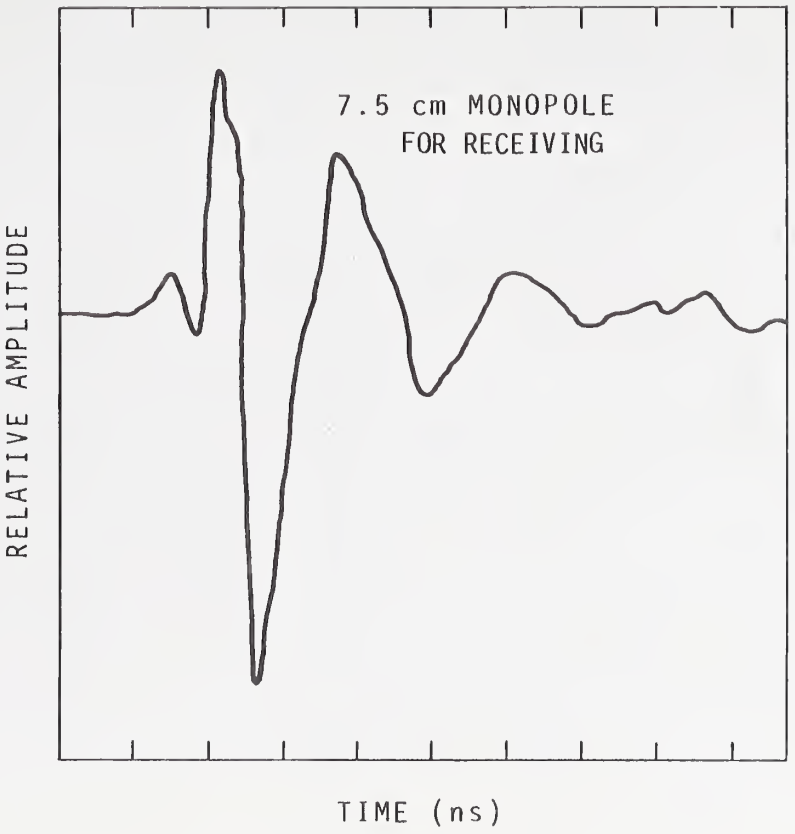

Figure 11. Time domain impulse responses.

b) a metal monopole

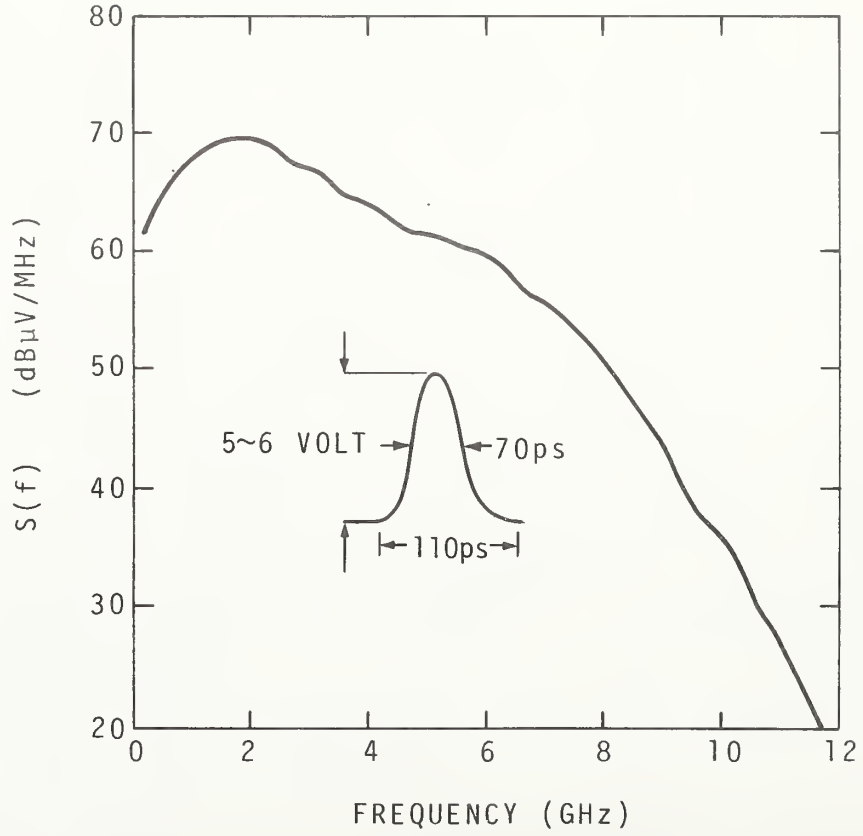

Figure 12. Spectrum amplitude of impulse.

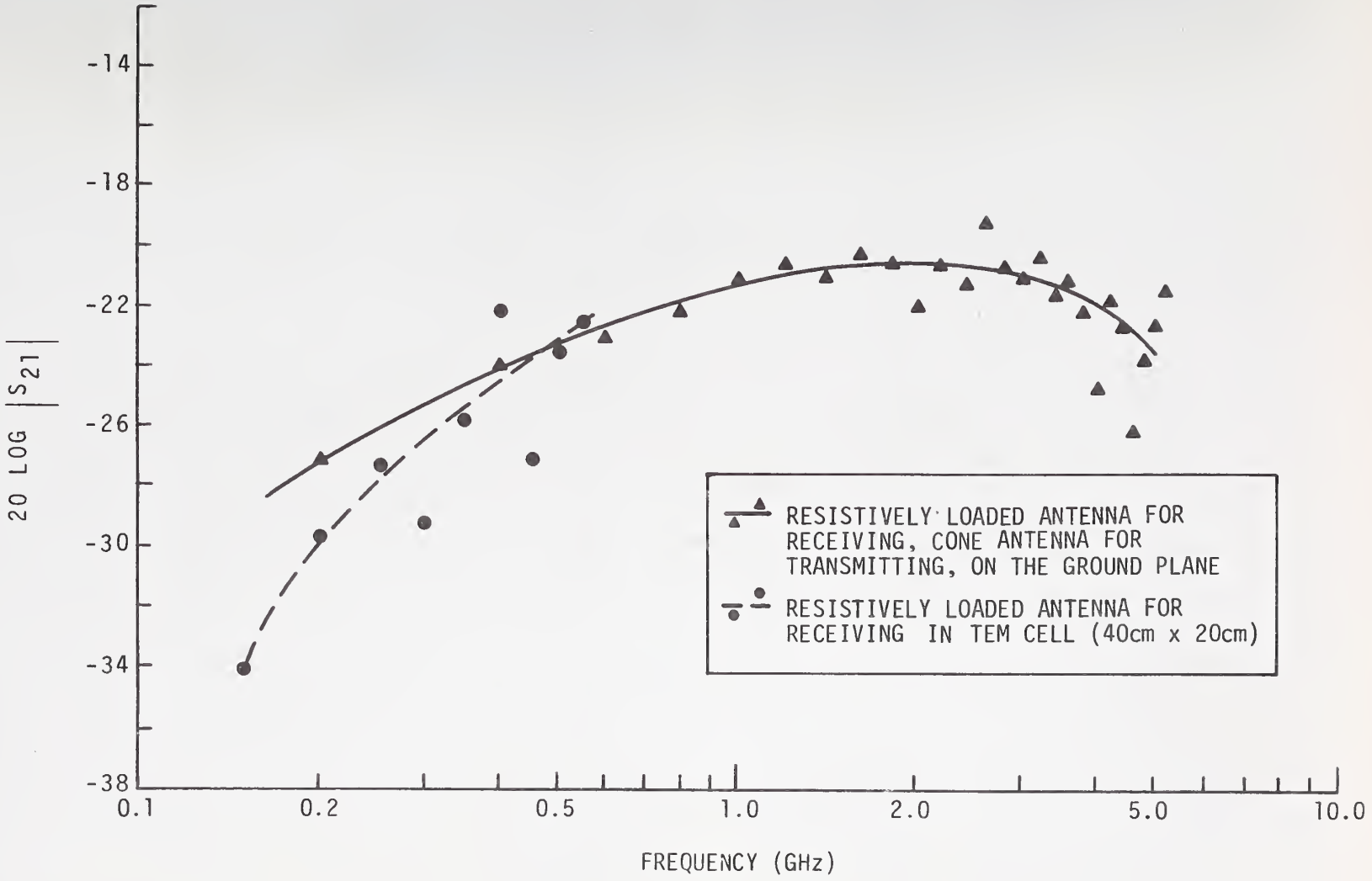

Figure 13. Transfer function of two antennas: conical standard antenna for transmitting and resistively loaded monopole for receiving.

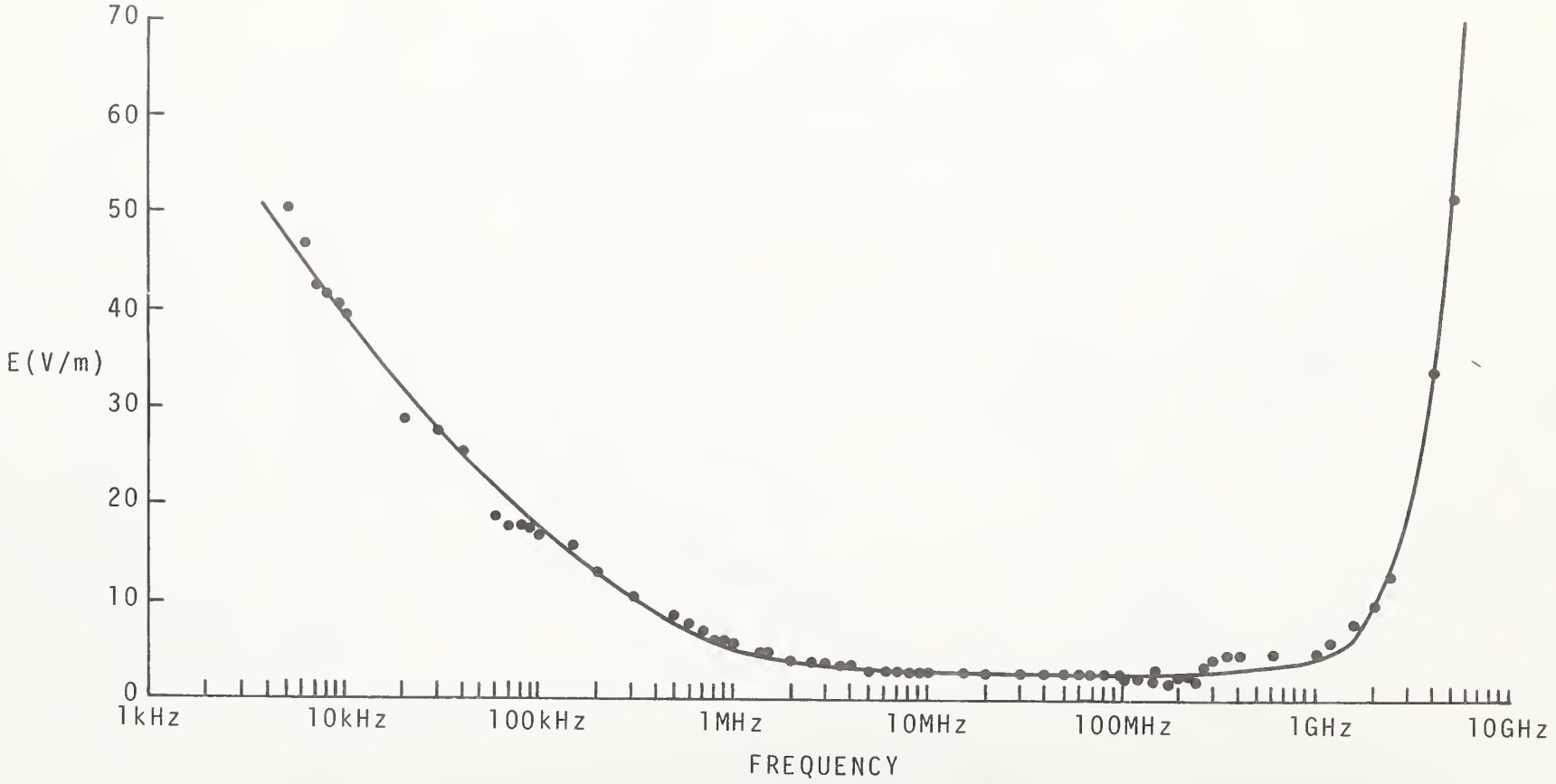

Figure 14. Frequency response of resistively loaded antenna.

NBS-114A (REV. 7-73)

U.S. DEPT. OF COMM. BIBLIOGRAPHIC DATA SHEET	1. PUBLICATION OR REPORT NO. NBSIR 77-861	2. Gov't Accession No.	3. Recipient's Accession No.

4. TITLE AND SUBTITLE

A RELATIVELY SHORT CYLINDRICAL BROADBAND ANTENNA WITH TAPERED RESISTIVE LOADING FOR PICOSECOND PULSE MEASUREMENTS

5. Publication Date
August 1977

6. Performing Organization Code
276.03

7. AUTHOR(S)
Motohisa Kanda

8. Performing Organ. Report No.

9. PERFORMING ORGANIZATION NAME AND ADDRESS

NATIONAL BUREAU OF STANDARDS
DEPARTMENT OF COMMERCE
WASHINGTON, D.C. 20234

10. Project/Task/Work Unit No.
2763495

11. Contract/Grant No.

12. Sponsoring Organization Name and Complete Address (*Street, City, State, ZIP*)

SAME AS ITEM 9.

13. Type of Report & Period Covered

14. Sponsoring Agency Code

15. SUPPLEMENTARY NOTES

16. ABSTRACT *(A 200-word or less factual summary of most significant information. If document includes a significant bibliography or literature survey, mention it here.)*

A relatively short cylindrical antenna with continuously tapered resistive loading has been studied for the purpose of picosecond pulse and extremely broadband CW measurements. The antenna considered is a non-conducting (glass) cylinder with continuously deposited, varying-conductivity, resistive loading. The current distributions on the antenna were numerically calculated using the method of moments. Using these current distributions, other quantities, such as input impedance, near-field and far-field radiation patterns, and radiation efficiency, were also numerically calculated and compared with the results using Wu-King's approximate current distribution. Agreement is relatively good except at high frequencies, $kh > \frac{\pi}{2}$, where the method of moment appears to give better results. To verify the theoretical results, several resistively loaded antennas were fabricated, and their picosecond pulse and extremely broadband CW receiving characteristics were analyzed for the frequency range between 5 kHz and 5 GHz. The experimental results indicate excellent linear amplitude and phase response over the frequency range. This provides the unique capability of this antenna to measure fast time-varying electromagnetic fields with minimal pulse-shape distortion due to nonlinear amplitude of phase characteristics.

17. KEY WORDS *(six to twelve entries; alphabetical order; capitalize only the first letter of the first key word unless a proper name; separated by semicolons)*

Broadband antenna; measurements; picosecond pulse; resistive loading, the method of moments.

18. AVAILABILITY

[X] Unlimited

[ ] For Official Distribution. Do Not Release to NTIS

[ ] Order From Sup. of Doc., U.S. Government Printing Office Washington, D.C. 20402, SD Cat. No. C13

[XX] Order From National Technical Information Service (NTIS) Springfield, Virginia 22151

19. SECURITY CLASS (THIS REPORT)	21. NO. OF PAGES
UNCLASSIFIED	45
20. SECURITY CLASS (THIS PAGE)	**22. Price**
UNCLASSIFIED	$4.00

INSTRUCTIONS

FORM NBS-114A: BIBLIOGRAPHIC DATA SHEET (REVERSE SIDE). This Bibliographic Data Sheet is an NBS adaptation of the form prescribed by COSATI guidelines (Appendix F. NBS Manual for Scientific and Technical Communications). Please complete with extreme care. This sheet will provide the basis for the literature citation of the publication, and in most cases it will become an integral part of the final publication itself.

A. Complete item 1 if information is available; otherwise, OTP will complete later. If non-NBS publication, state:"see item 15". (Additional instructions under K below.)

B. Ignore items 2, 3, 6, and 14; these are reserved for possible future use.

C. Complete items 4 and 7. When NBS-114A is resubmitted these items must be as they will actually appear on the published paper.

D. Leave items 5, 21, and 22 blank; OTP will complete.

E. Items 9, 19, and 20 are preprinted; you need add nothing.

F. Complete items 10, 11, and/or 12 when applicable. If no sponsor is involved, in item 12 state: same as item 9.

G. For item 13, enter "Final" or "Interim" and calendar period covered, as appropriate.

H. For item 15, enter other relevant information. (For example, upon receipt of completed Form NBS-266 from author, OTP will enter the complete citation for NBS-authorized papers published in non-NBS media.)

I. Complete items 16 and 17. Guidance is given in Section 4 and Appendix B of the NBS Manual for Scientific and Technical Communications. The abstract must agree with the one of the published paper.

J. For item 18, indicate one of the following: "Unlimited" - for open-literature documents cleared under NBS editorial procedures, or "For official distribution. Do not release to NTIS" - for limited, restricted, or need-to-know material. (See 5.1.4.2.1 of Brady memo dated January 16, 1973 "Reports to Sponsors.")

K. In completing item 1, use the brief designators shown in the right-hand column below. Each designator will be followed by the specific publication number for that item. This number will be the same in both the longer and briefer designators for the same document. For example: NBS Technical Note 548 will be equivalent to NBS TN-548. You would enter NBS TN-548 in item 1 of Form NBS-114A.

NBS Identification	
NBS Technical Note	NBS TN-
NBS Monograph	NBS MN-
NBS Handbook	NBS HB-
NBS Special Publication	NBS SP-
NBS Applied Mathematics Series	NBS AMS-
NBS National Standard Reference Data Series	NBS NSRDS-
NBS Building Science Series	NBS BSS-
NBS Federal Information Processing Standards Publication	NBS FIPS-
NBS Voluntary Product Standards	NBS PS-
NBS Consumer Information Series	NBS CIS-
NBS Journal of Research Section A	NBS JRA-
NBS Journal of Research Section B	NBS JRB-
NBS Dimensions	NBS D-
NBS Interagency or Internal Report *	NBS IR-

Since each paper in the two volume NBS Journal of Research is assigned a specific designator, OTP will add appropriate Journal designator for item 1.

*If the outside sponsor assigned his own number, enter his number in item 1, and the NBSIR number in item 8.